Environ Fluid Mech (2008) 8:281–312
DOI 10.1007/s10652-008-9084-5

ORIGINAL ARTICLE

Evaluation of the QUIC-URB fast response urban wind model for a cubical building array and wide building street canyon

Balwinder Singh · Bradley S. Hansen · Michael J. Brown · Eric R. Pardyjak

Received: 21 January 2008 / Accepted: 17 July 2008 / Published online: 28 August 2008

Abstract This paper describes the QUIC-URB fast response urban wind modeling tool and evaluates it against wind tunnel data for a 7×11 cubical building array and wide building street canyon. QUIC-URB is based on the Röckle diagnostic wind modeling strategy that rapidly produces spatially resolved wind fields in urban areas and can be used to drive urban dispersion models. Röckle-type models do not solve transport equations for momentum or energy; rather, they rely heavily on empirical parameterizations and mass conservation. In the model-experiment comparisons, we test two empirical building flow parameterizations within the QUIC-URB model: our implementation of the standard Röckle (SR) algorithms and a set of modified Röckle (MR) algorithms. The MR model attempts to build on the strengths of the SR model and introduces additional physically based, but simple parameterizations that significantly improve the results in most regions of the flow for both test cases. The MR model produces vortices in front of buildings, on rooftops and within street canyons that have velocities that compare much more favorably to the experimental results. We expect that these improvements in the wind field will result in improved dispersion calculations in built environments.

Keywords Wind model · Fast-response · Urban dispersion modeling · Street canyon

1 Introduction

Airborne releases of toxic gases and aerosols may occur in cities and cause great harm to the general population. Recent field experiments (e.g., New York City [26]; Oklahoma City [2]; Salt Lake City [1]) and computational fluid dynamics modeling [14,16,27,46] of tracer releases in built-up city centers indicate that the buildings significantly alter transport and

B. Singh · B. S. Hansen · E. R. Pardyjak (✉)
Department of Mechanical Engineering, University of Utah, Room 2110, Salt Lake City, UT 84112, USA
e-mail: pardyjak@eng.utah.edu

M. J. Brown
Los Alamos National Laboratory, Los Alamos, NM 87545, USA

dispersion. Near street level, for example, the plume may travel several blocks in a direction opposing the prevailing wind and many blocks laterally. This topological dispersion can lead to secondary sources and significantly alter the rate of lateral dispersion [6]. A ground-level source can rise several hundred meters in depth in less than a block when caught in the updraft just downwind of a tall building [27]. Buildings also alter the timing of the transport and dispersion, generally resulting in much longer residence times as compared to open terrain [17,28].

For applications where quick turn-around time is required (e.g., an emergency response to a chemical accident in a city) or where thousands of simulations must be performed in a few days or less (e.g., a vulnerability assessment of a particular urban site), computational fluid dynamics (CFD) modeling is currently not fast enough. While "on demand" CFD calculations are not practical for these applications, there are a number of research groups investigating the use of computational fluid dynamics (CFD) models for fast response applications. Ideas range from coarse resolution simulations using drag [13,38] to library approaches where a large number of cases are pre-computed and results for specific cases are interpolated from the library [46,54].

For many years, "urbanized" Gaussian plume models have been used for quick turn-around applications using urban vertical and lateral plume spread parameters [39]. Evaluation studies have shown that at distances greater than about one kilometer from the source and/or for low density urban areas Gaussian models perform fairly well when comparing maximum concentrations that are unpaired in space [25,58]. Since Gaussian plume models only use a single wind speed and wind direction as input, they cannot represent the complex three-dimensional wind and concentration fields that develop within the urban core around buildings. To better account for the effects of buildings on near source transport and dispersion, a number of researchers have developed simple fast-running models to account for the lateral displacement of a plume centerline due to off-axis channeling [57] and to compute the concentration fields around a single isolated building [20,47,52,62] and within a street canyon [7,15,18,63]. These models are capable of predicting dispersion for isolated buildings, two building street canyons, or for idealized building arrays, but not for the complex arrangements and shapes of buildings that occur in real cities.

Over the past 10–15 years, there has been a considerable amount of effort placed in developing urban transport and dispersion models that run relatively fast but account for the effects of groups of arbitrary shapes and arrangements of buildings in an approximated way. Hall et al. [24] describe a Gaussian puff model called the Urban Dispersion Model (UDM) for use on neighborhood to city scales ($\sim$10 m to 10 km). The model accounts for building wake cavity mixing and some along street channeling, but does not compute a 3D flow field around the buildings. When a puff intercepts a building, it is instantaneously placed in the lee of the building in the cavity and puffs are then emitted over time from the cavity. Brook et al. [10] have evaluated the model against idealized building arrays in the lab and field as well as against outdoor urban field experiment data. Another well known, but non-peer reviewed modeling system, called MIDAS-AT, computes 3D wind fields around building complexes using potential flow theory with dispersion modeled using a traditional three-term boundary-layer random-walk model (http://www.absconsulting.com/midas/). The potential flow approach allows for channeling of the flow down streets, but does not allow for important rotational flow phenomena such as street canyon vortices that form between buildings or recirculating cavities that develop downwind of an isolated building.

Röckle [48] derived a unique model that computes flow around buildings using empirical equations and mass conservation. Röckle's methodology was incorporated into the ABC and ASMUS models which were intended for dispersion applications at industrial sites and have

undergone several evaluation studies [22,23]. The ABC and ASMUS models accomplished transport and dispersion through a K-theory Eulerian diffusion model. A small number of urban wind models have been developed based on the Röckle approach which have all utilized Lagrangian random-walk models to accomplish transport and dispersion [34,41,59]. Our team has also utilized the Röckle concept. Over the past 5 years, we have worked to carefully evaluate the model, improve the original flow algorithms and implement new algorithms. The wind model has been modified to work with complex arrangements of buildings including the ability to stack buildings on top of one another to create semi-realistic city center layouts. This article and Gowardhan et al. [21] represent the first peer-reviewed descriptions of the model. The Gowardhan et al. [21] paper focuses on flow around individual buildings, while this paper investigates flow through groups of buildings. The wind model, QUIC-URB, is part of the Quick Urban & Industrial Complex (QUIC) dispersion modeling system which contains an "urbanized" random-walk model called QUIC-PLUME and a graphical user interface called QUIC-GUI. QUIC-PLUME is unique in that it contains a non-local mixing scheme and more drift terms than the traditional random-walk model in order to account for the inhomogeneous turbulence associated with urban flows [60]. QUIC has been applied to neighborhood-scale problems in such places as New York City, Washington DC, Chicago, Oklahoma City and Salt Lake City (see for example: http:/www.lanl.gov/projects/quic/).

In this paper, our purpose is to evaluate the QUIC-URB wind model against mean velocity measurements obtained in a wind tunnel at fairly high spatial resolution for an incident flow normal to a 7×11 array of cubes. A new street canyon algorithm for flow normal to street canyons is presented and compared to the standard Röckle model. We also evaluate QUIC-URB against wind tunnel data obtained for a street canyon region formed between two wide buildings. Although a number of evaluation studies have been performed looking at the performance of Röckle-style modeling systems using concentration measurements from tracer experiments, relatively few detailed evaluations have included high resolution wind measurements. We begin this paper by describing the QUIC-URB wind model, including the standard Röckle street canyon algorithm. This section is followed by a brief description of the 7×11 building array wind-tunnel experiment. The wind tunnel data for the 7×11 building array are compared with the standard Röckle algorithms to highlight the shortcomings of these algorithms. In the next sections, we describe the changes that our team has made to the building flow algorithms and in the results section we compare the QUIC-URB model output to the velocity measurements of 7×11 building array as well as a wide buildings street canyon data set using both the original Röckle algorithms and our new algorithms.

2 QUIC-URB model description

The modeling strategy adopted in QUIC-URB was originally developed by Röckle [48] and uses a 3D mass consistent wind model to explicitly resolve time-averaged wind fields around buildings. The mass consistent technique is based on Sherman's [53] 3D complex terrain diagnostic wind model. The basic methodology involves generating an initial wind field ($\vec{V}^o = u^o\hat{i} + v^o\hat{j} + w^o\hat{k}$) that includes various empirical parameterizations to account for the physics of flow around buildings and then forcing this velocity field to be divergence free subject to the weak constraint that the variance of the difference between the initial velocity field and mass consistent final velocity field ($\vec{V} = u\hat{i} + v\hat{j} + w\hat{k}$) is minimized. This is done using a general variational analysis formalism originally developed by Sasaki [49–51] in which Eq. 1 is minimized.

$$E(u,v,w,\lambda) = \int_V \left[\alpha_1^2\left(u-u^o\right)^2 + \alpha_1^2\left(v-v^o\right)^2 + \alpha_2^2\left(w-w^o\right)^2 + \lambda\left(\frac{\partial u}{\partial x}+\frac{\partial v}{\partial y}+\frac{\partial w}{\partial z}\right)\right] dxdydz \tag{1}$$

In Eq. 1, λ's are Lagrange multipliers (with units of inverse time) and α_i's are Gaussian precision moduli (weighting factors with units of inverse velocity). As noted by Kaplan and Dinar [34], α_i are variables that enhance or restrict the correction of the wind components with respect to each other. In QUIC-URB, single building tests [3] confirmed that for most cases $\alpha_i = 1$ produces optimal results in neutral stability flows.

The velocity field is updated using the Euler–Lagrange equations whose solution minimizes Eq. 1. Namely,

$$u = u^o + \frac{1}{2\alpha_1^2}\frac{\partial \lambda}{\partial x} \tag{2a}$$

$$v = v^o + \frac{1}{2\alpha_1^2}\frac{\partial \lambda}{\partial y} \tag{2b}$$

$$w = w^o + \frac{1}{2\alpha_2^2}\frac{\partial \lambda}{\partial z} \tag{2c}$$

These equations are subject to the boundary conditions $\partial\lambda/\partial n = 0$ at a solid boundary (where n is the outward normal direction) and $\lambda = 0$ at inflow/outflow boundaries. An equation for λ is obtained by differentiating Eq. 2 and substituting the result into the continuity equation for the final velocity field, $\nabla \cdot \vec{V} = 0$ [53]. This procedure results in the following Poisson equation that can easily be solved for λ using the specified boundary conditions:

$$\frac{\partial^2\lambda}{\partial x^2} + \frac{\partial^2\lambda}{\partial y^2} + \left(\frac{\alpha_1}{\alpha_2}\right)^2\frac{\partial^2\lambda}{\partial z^2} = -2\alpha_1^2\left(\frac{\partial u^o}{\partial x}+\frac{\partial v^o}{\partial y}+\frac{\partial w^o}{\partial z}\right). \tag{3}$$

In QUIC-URB, Eq. 3 is solved using a simple iterative successive over-relaxation or SOR solver [45] on a non-uniform staggered grid where velocities are face center values and Lagrange multipliers are cell-centered quantities.

The ability of the QUIC-URB model to produce accurate wind fields around buildings is dependent on the empirical wind parameterizations. These parameterizations introduce rotation into the flow field and without these parameterizations the method is essentially a potential flow solver. The upwind boundary-layer profile may be specified as a power-law, log-law, urban canopy, or user-specified profile. This profile is applied uniformly in portions of the domain that are not affected by building flow features. For problems in which the flow varies spatially outside of the urban area (e.g., complex terrain), multiple data profiles or point measurements can be assimilated to produce a spatially-varying wind field [8]. As described by Gowardhan et al. [21], for isolated buildings, QUIC-URB utilizes a number of empirical building algorithms for determining the initial wind fields of the vortex regions associated with: the building rooftop [4,43], the upstream recirculation zone [5] and the downwind recirculation cavity and the velocity deficit wake [48]. Details of these models are given in Gowardhan et al. [21], but here we highlight a few points relevant to this test case. The standard Röckle upstream recirculation zone model is an elliptical volume with all initial velocity field components specified to be zero. For flow normal to a building face, the improved QUIC-URB model separates the region upstream of the building into two elliptical regions: a displacement zone where the velocities are reduced and a recirculation zone where

the velocities are specified to form a vortex. The original Röckle formulation did not contain a rooftop recirculation parameterization to account for separation at the leading edge of a building. The complete details of the improved QUIC-model are described in Gowardhan et al. [21] for both normal and off-angle winds. For normal incident winds, a rooftop vortex region is specified following Wilson [61]. The velocity field in the vortex is applied uniformly across the width of the rooftop, and takes on a maximum negative value just above the building rooftop and then increases monotonically to the upstream boundary layer velocity at the top of the cavity zone. The improved QUIC-model includes a rooftop recirculation region with logic to determine when a rooftop recirculation cavity is necessary. This is quite important for groups of buildings. For example, in the 7×11 test case presented here, only the buildings in the first row have a rooftop recirculation zone. For flow normal to a building face, the rooftop algorithm logic always applies a rooftop cavity if the building is isolated and far from other buildings or if the building is greater in height than the nearby upwind building.

2.1 Standard Röckle street canyon model

In this section, we describe our implementation of the Röckle [48] street canyon (SC) algorithm for urban flows with multiple buildings (hereafter referred to as SR for standard Röckle model). The empirical SC algorithm accounts for the generation of a classical SC vortex that forms between two closely spaced buildings [42]. While 3D SC flow is extremely complicated, it is convenient (and conventional) to break the flow into three phenomenological flow regimes based on the spacing between the buildings: isolated roughness flow, wake interference flow and skimming flow [31]. Following the notation in Fig. 1 these regimes roughly correspond to cubical building ratios of spacing (S) to building height (H) of about: $S/H > 2.5$, $1.4 < S/H < 2.5$ and $S/H < 1.4$ respectively [42]. Because the wake interference flow regime is unsteady and difficult to parameterize, Röckle assumed that the canyon flow could be simply modeled by two flow regimes: skimming and isolated flow. The decision criteria used to determine which flow regime to implement is based on a non-dimensional building spacing parameter that is a function of street canyon and building geometries. In our implementation, canyon flow is parameterized by two flow regimes similar to Kaplan and Dinar [34]: skimming (when $S/H < 1.25 + 0.15\,(W/H)$ for $W/H < 2$ and $S/H < 1.55$ for $W/H \geq 2$) and isolated flow $S/H > 1.25 + 0.15\,(W/H)$, where W is the crosswind width of the building. In the isolated flow regime, parameterizations for the upwind, rooftop, and wake cavities are applied in the same manner as for the case when there are no other buildings in the domain. In the skimming regime, a reverse flow is imposed between the buildings below roof level (see Fig. 1a, b). The imposed reverse flow interacts with the boundary layer flow at the sides of the street canyon to form two counter rotating vortices. The streamwise initial velocity specification for the reverse flow within the canyon is given by

$$\frac{u^o(x, y, z)}{u^o\,(H)} = -\frac{x_{\text{can}}}{(0.5S)}\left(\frac{S - x_{\text{can}}}{0.5S}\right), \tag{4}$$

and the vertical component is given by

$$\frac{w^o(x, y, z)}{u^o\,(H)} = -\left|\frac{1}{2}\left(1 - \frac{x_{\text{can}}}{0.5S}\right)\right|\left(1 - \frac{S - x_{\text{can}}}{0.5S}\right). \tag{5}$$

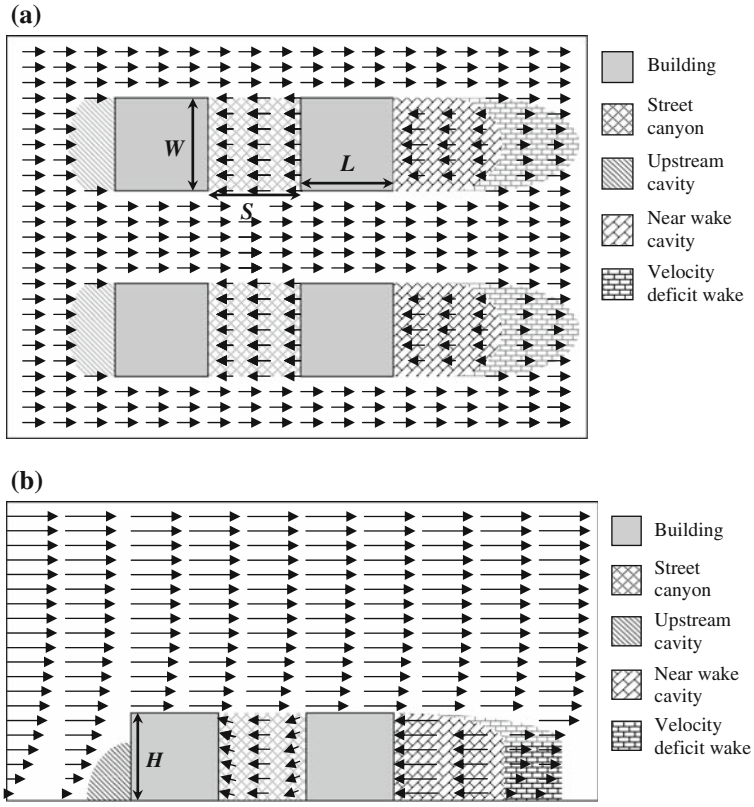

Fig. 1 Schematic showing the various flow regions and initial velocity field (prior to mass conservation) associated with the Röckle parameterizations in (**a**) the horizontal and (**b**) vertical planes for normal flow

Here, x_{can} is the distance from the backwall of the upwind building, and the other parameters are defined in Fig. 2.

For flow that is not normal to the SC, the velocity component normal to the axis of the SC is specified by Eq. 4 and the component parallel to the SC is left unchanged, resulting in a "channeling velocity." The next section describes the SR model evaluation against the wind tunnel data and highlight the various shortcomings present in the SR model.

3 Evaluation of the standard Röckle model against a 7 × 11 building array wind-tunnel data set

3.1 Wind-tunnel experiment description

The experiments were carried out in a 3.7 m wide, 2.1 m high, and 18.3 m long open-return meteorological wind tunnel at the U.S. Environmental Protection Agency's Fluid Modeling Facility [55]. The cubical building array examined in this study consisted of 11 rows of blocks in the streamwise direction and seven columns of blocks in the crosswind direction (Fig. 3). The building array was oriented perpendicular to the inflow wind. The blocks were

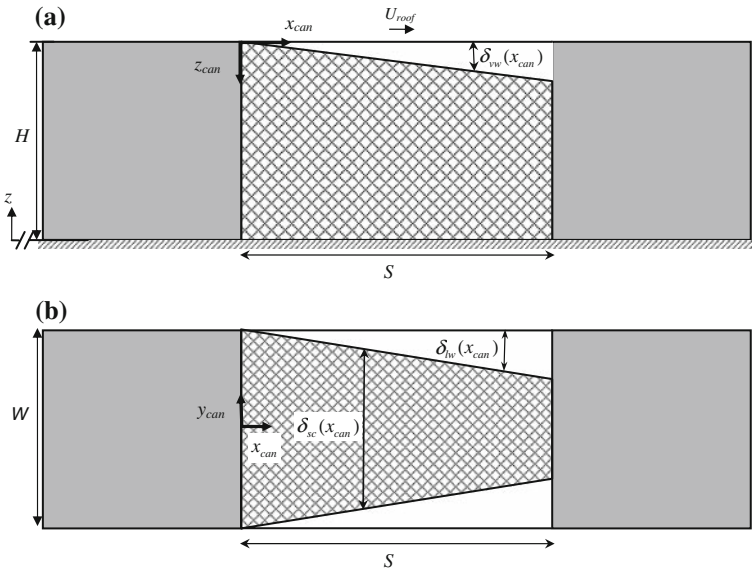

Fig. 2 Schematic showing the notation and local coordinate system for the modified Röckle (MR) street canyon model (**a**) side view and (**b**) plan view

of equal height, width and length ($H = W = L = 150\,\text{mm}$) and were spaced $S = H$ apart in the along-wind and cross-wind directions. As discussed above, with a space-to-height (S/H) ratio of unity, the 7×11 array of cubes should be in the skimming flow regime [42]. The building models were immersed in a simulated 1.8 m deep neutral atmospheric boundary layer which was created using spires near the tunnel entrance [32] and floor roughness elements. Using a length scale equal to H and a reference velocity of $3\,\text{ms}^{-1}$ at $z = H$, the Reynolds number was approximately 30,000, well above the critical value required for Reynolds number independence [12,56]. The building height was less than 10% of the boundary-layer depth, similar to the ratio in real downtown areas. While no specific scale ratio was chosen, a representative value would be 250:1, hence the building models would correspond to full-scale buildings on the order of 30–40 m in height.

A hot-wire anemometer with an X-array sensor was used to measure the mean velocity and turbulence intensity profiles of the approach flow in the absence of any buildings. To account for reversed flow and high turbulence intensity within the building array, measurements were made with a pulsed-wire anemometer (PWA, Bradbury and Castro [9]). All PWA measurements were obtained using a pulsing rate of 10 Hz and an averaging time of 120 s at each measurement location. More information on the experiment can be found in Lawson et al. [37] and Brown et al. [11].

3.2 Description of the model test case

In the section that follows, the standard Röckle (SR) model is compared to the wind-tunnel data described in Sect. 3.1. Matching the inlet profile proved to be somewhat difficult because a 500 mm smooth wall gap existed between the upstream roughness elements and the start of the 7×11 array in the wind tunnel. In this region, the experimental data

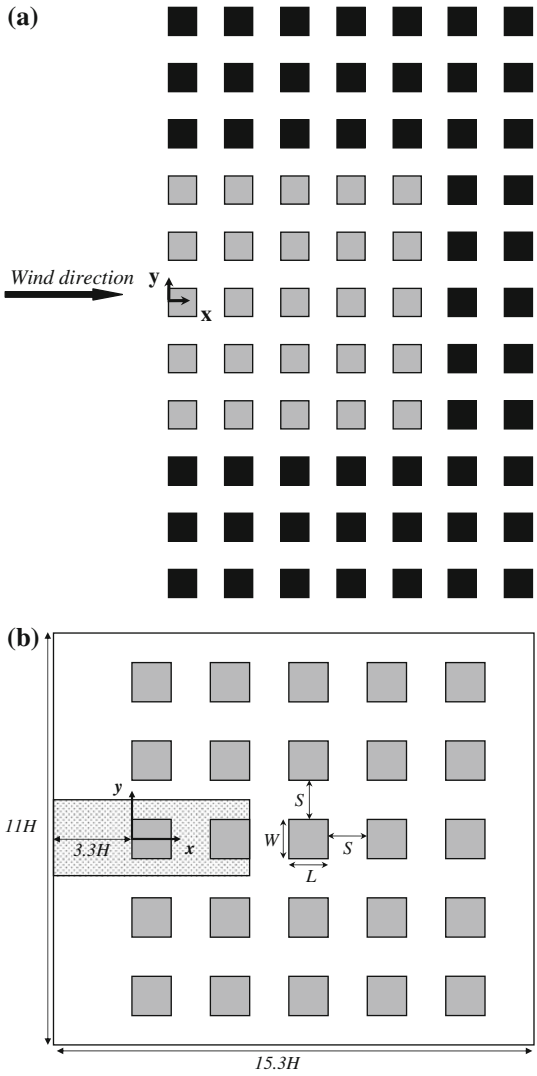

Fig. 3 A schematic of the 7×11 building array used in the wind-tunnel study is shown in panel (**a**). The subset of gray buildings in panel (**a**) are also shown in panel (**b**) which is an enlargement showing the 5×5 building array used in the QUIC-URB simulations. In panel (**b**), the gray highlighted area in the first two columns at the center of the computational domain is the region where comparisons have been made between the model and the wind-tunnel data

showed the development of an internal boundary layer that QUIC-URB is unable to simulate. Hence, the inlet profile was specified at $x/H = -3.3$ such that the solution matched the experimental data at $x/H = -1.5$ as closely as possible. To match the data, the inlet velocity profile was specified to be logarithmic with a roughness length of 2 mm and a reference velocity $U_{\text{ref}} = 2.82\,\text{ms}^{-1}$ at the building height ($H = 0.15\,\text{m}$). Figure 4 shows the comparison of the velocity profile from the model and the experimental data at $x/H = -1.5$. The profile is described well with the logarithmic fit shown (2.2% RMS error). The boundary conditions on the velocity at the inlet, outlet and along the top of the domain are Dirchlet and specified by the initial logarithmic profile. While QUIC has a variable grid resolution capability, the simulations were run with a uniform grid resolution of 0.015 m such that the buildings were resolved with 10 cells in each direction. Simulations were also run at double and half of this resolution and the results for the finer grid were quite similar ($<1\%$ difference in RMS error) to the 0.015 m grid.

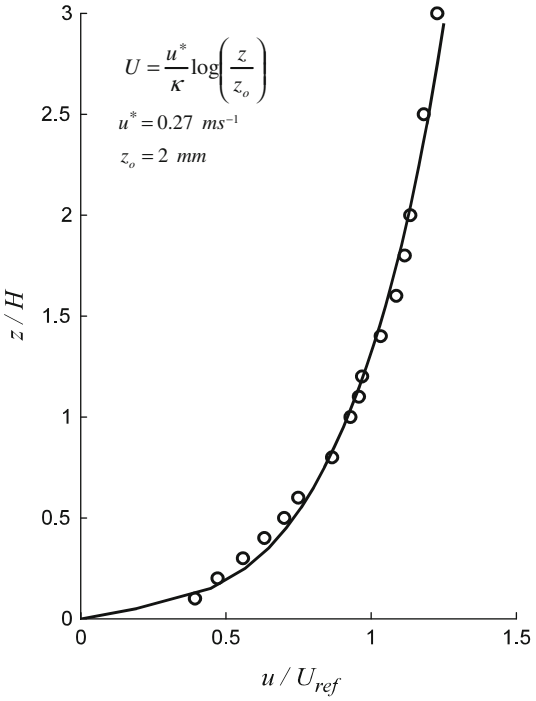

Fig. 4 Inflow profile comparison between the experimental data and the logarithmic velocity profile used to initialize QUIC-URB at $x/H = -1.5$

The experimental measurements were made in a subset of the 7×11 array. The region where measurement comparisons have been made to the simulations is highlighted in Fig. 3b. Experience with the type of diagnostic urban wind model discussed here indicates that the last column of buildings on either side of the array does not affect the simulated centerline velocities. Hence, these buildings have been omitted from the simulations and the building array of 5×5 (25 buildings) shown in Fig. 3b was used for all of the simulations. The domain size used for the simulations was 2.295 m $\times$ 1.650 m $\times$ 0.450 m ($153 \times 110 \times 30$ in grid cell units) in the x, y and z directions respectively. The test case presented here took $\sim$26 s to run on a 2.4 Ghz Intel Core 2 Duo Processor with 2 GB of random access memory (RAM).

3.3 Standard Röckle model evaluation—7×11 array

In this section, we evaluate the performance of the SR model qualitatively by comparing general flow features. Figure 5a shows a velocity vector comparison between the experimental data and the SR model in the vertical plane along the centerline at the beginning of the building array. The SR model does a reasonably good job of predicting the location of the stagnation point on the upwind face of the first-row building ($z/H \sim 0.7$). The experimental data reveal a small, but well-defined recirculation zone upstream of the first building, whereas the SR model results in a large unorganized cavity with no well-defined features (Fig. 5a, b).

The experimental data suggest that a recirculation zone may exist above the rooftop of the first building (Fig. 5a). As expected, the SR model—which does not contain a rooftop recirculation scheme—overestimates the streamwise velocity above the rooftop.

Looking at the flow in the first street canyon (Fig. 5a), the SR model produces somewhat stronger downdrafts and backflow as compared to the experimental data. Moreover,

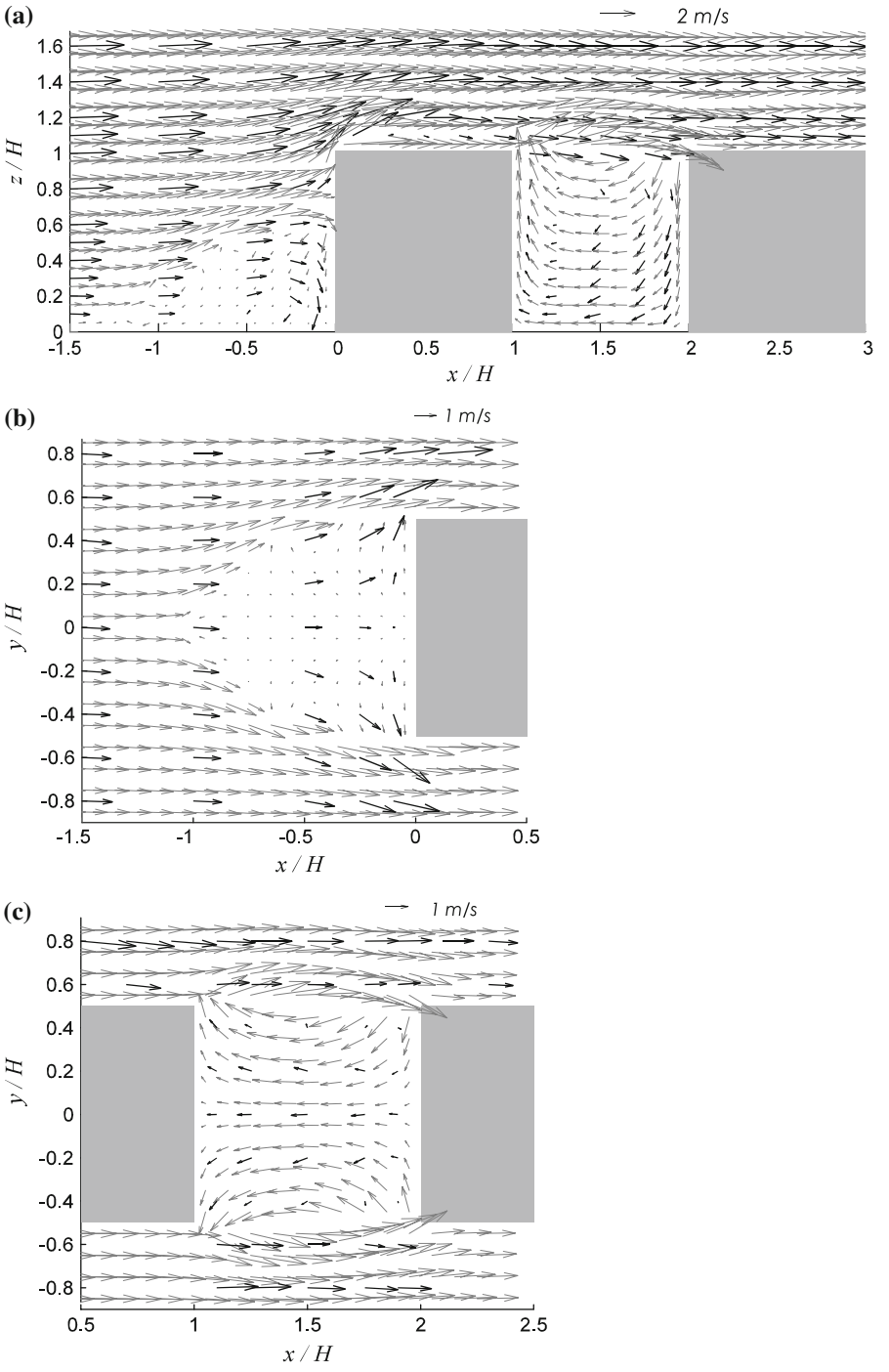

Fig. 5 Comparison of the SR model-computed velocity vectors (gray) with the experimental measurements (black) (**a**) in the x–z plane along the building centerline, (**b**) in the x–y plane at $z/H = 0.2$ upwind of the central building in the first row and (**c**) in the x–y plane at $z/H = 0.2$ in the first row street canyon

the center of the SC vortex simulated by our implementation of the SR model is raised well above the height yielded in the experimental data. The SR scheme results in winds that too quickly revert to the purely horizontal flow above the canyon, whereas the measurements show a significant downward component at the midpoint of the canyon. Figure 5c depicts the wind patterns in the first canyon near ground level at $z/H = 0.2$. The SR scheme generates counter-rotating vortices in agreement with the measurements however, the modeled winds are too strong and the vortex centers are too close to the street canyon ends as compared to the experimental data.

4 Modified Röckle street canyon model

To address the various shortcomings present in our implementation of the SR model, a modified Röckle street canyon model (hereafter referred to as MR for modified Röckle model) has been developed and evaluated prior to incorporating it into the operational version of the QUIC modeling system. Our implementation of the SR model does not account for diffusion of streamwise momentum into the SC from aloft resulting in a sharp transition between the street canyon velocity and the air aloft. It also tends to over predict the velocities within the central part of the canyon. The modified SC algorithm for the skimming flow regime suggested here extends the Röckle model to include parameterizations that more effectively approximate the physics observed in field and wind-tunnel data. As shown in Figs. 2 and 6, the SC is broken up into three physically-based regimes: (i) a central canyon region dominated by the classical SC vortex, (ii) a vertical turbulent diffusion region associated with the transport of momentum into and out of the canyon from above, and (iii) a horizontal turbulent diffusion region associated with the lateral transport of momentum into and out the canyon. The vertical and horizontal diffusion regions are defined by triangular prisms or wedges that extend from the leeward edge of the upstream building. Conceptually, the flow within each of these wedges is modeled as a single stream shear layer (or mixing layer). The width of the mixing region within plane mixing layers is well known to grow linearly with distance downstream of the start of the layer and to have a velocity profile that takes on a hyperbolic tangent shape [44]. We use these physically-based concepts to develop a model for the mixing region at the edges of the SC.

As illustrated in Fig. 2, the vertical wedge is a right-angled wedge with length S, and maximum height, $\delta_{vw}|_{x_{\text{can}}=S} = 0.2S$ [44]. The vertical wedge extends across the entire width W of the street canyon. Within the wedge, the velocity is specified to behave similar to a classical single-stream shear layer and is given by the following hyperbolic tangent model [40]:

$$\frac{u^o(x, y, z)}{U_{\text{roof}}} = \frac{\tanh\left[\left(\delta_{vw}\left(x_{\text{can}}\right) - z_{\text{can}}\right)/\delta_{vw}\left(x_{\text{can}}\right)\right]}{\tanh(1.0)}. \tag{6}$$

Here, the vertical wedge depth $\delta_{vw}(x_{\text{can}}) = 0.2x_{\text{can}}$ is a linear approximation to the depth of the shear layer. U_{roof} is a reference velocity in the streamwise direction obtained by generating a displaced logarithmic profile over the canyon. The displacement height (d) is taken as the height of the shortest building making up the street canyon and the reference wind direction is given by the local wind direction at the center of the canyon at rooftop level of the shortest building. We recognize that typical measured values of the displacement height are closer to $d/H \sim 0.7$ [33], however for modeling simplicity we use $d/H = 1$. Within the wedge, the vertical winds are specified to be zero. Currently, for flow that is not normal to the SC the MR model is identical to the SR model described above.

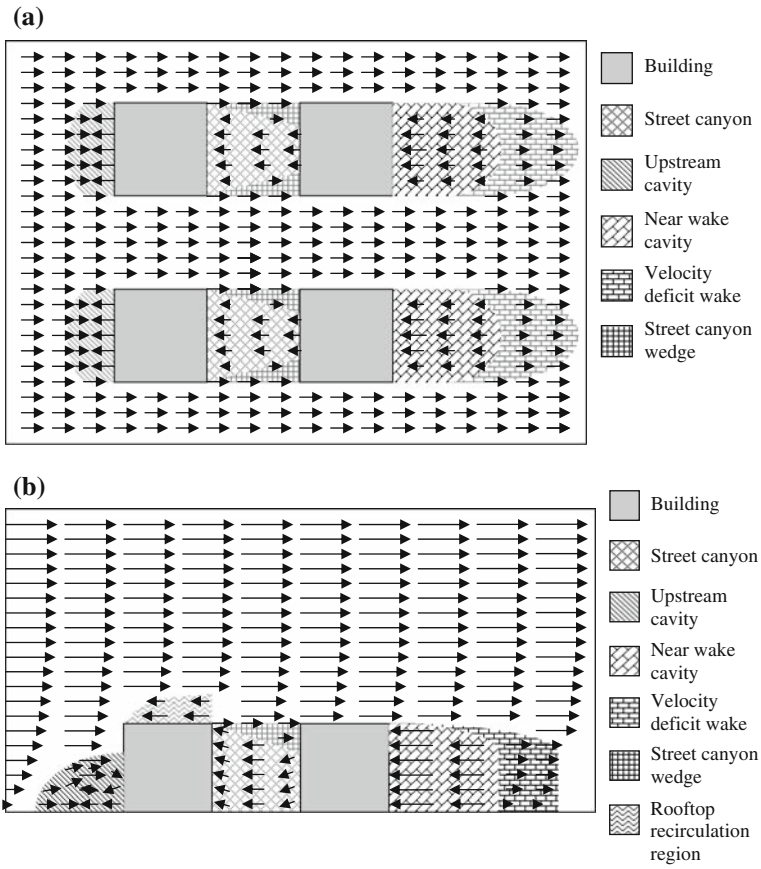

Fig. 6 Schematic illustrating the flow regions and initial velocity fields associated with the MR street canyon parameterization in (**a**) the horizontal and (**b**) vertical plane

Similarly, the lateral wedge is also a right angled wedge with maximum width $\delta_{lw}|_{x_{\text{can}}=S} = 0.2S$. The streamwise velocity in the shear layer is specified using the following hyperbolic tangent model:

$$\frac{u^o(x, y, z)}{u^o_{bl}(z)} = \gamma \left[\frac{\tanh\left[Y_{lw}/\delta_{lw}(x_{\text{can}})\right]}{\tanh(1.0)} \right]. \tag{7}$$

In Eq. 7, $u^o_{bl}(z)$ is the upstream boundary layer velocity that is unaffected by buildings and $\gamma = 0.3$ is a velocity reduction correction factor that has been empirically determined with the present 7×11 data set to account for the SR model's over prediction of the strength of the velocities in the canyon. $Y_{lw} = [|y_{\text{can}}| - \delta_{SC}(x_{\text{can}})/2]$, $\delta_{SC}(x_{\text{can}}) = W - 2\delta_{lw}(x_{\text{can}})$ and $\delta_{lw}(x_{\text{can}}) = 0.2x_{\text{can}}$, where $\delta_{lw}(x_{\text{can}})$ is the width of the lateral wedge. As in the vertical wedge, the vertical component of the velocity is set to zero.

As shown in Eqs. 4 and 5, the original SR model does not explicitly parameterize a lateral variation in the wind speed within the street canyon. Including a lateral diffusion wedge provides a smooth transition of the flow between the wedge and the street canyon interior (see cross hatched region in Fig. 2) that approximates the momentum diffusion process.

This lateral diffusion is accomplished by modeling the along-wind component of the velocity within the street canyon core to incorporate lateral variation:

$$\frac{u^o(x, y, z)}{u^o(H)} = -\gamma \frac{x_{\text{can}}}{(0.5S)} \left(\frac{S - x_{\text{can}}}{0.5S} \right) F_{SC}(y_{\text{can}}). \tag{8}$$

In Eq. 8, γ is the same velocity reduction factor from Eq. 7 and is applied throughout the canyon. F_{SC} is a continuously-varying function that reduces the velocity in the lateral direction with distance from the center of the canyon and is given by:

$$F_{SC}(y_{\text{can}}) = \left[1 - \frac{|y_{\text{can}}|}{\delta_{SC}(x_{\text{can}})/2} \right]^p. \tag{9}$$

The empirical coefficient p is a parameter that was adjusted to improve the final comparison with the 7×11 data set. The best match to the experimental data was obtained with the exponent p set to 0.25. Note that the algorithms are applied in sequential order: the central SC is calculated first, then the lateral wedge and finally the vertical wedge; in this process, the velocities computed with the later algorithms overwrite the earlier ones in regions of overlap. This new algorithm is only applied to flows that are near normal to the building face ($\pm 5°$). Within this range, the velocity component normal to the axis of the SC is specified by Eqs. 6–8 and the component parallel to SC is left unchanged, resulting in a "channeling velocity." Outside of this range, the model reverts to the SR model.

Another change that we have made to our implementation of the SR algorithm is a modification to the criteria to determine the existence of a street canyon; it is now based on the single building wake recirculation cavity length formula of Fackrell [19], namely

$$\frac{S^*}{H} = \frac{1.8 \frac{W}{H}}{\left(\frac{L}{H}\right)^{0.3} \left(1 + 0.24 \frac{W}{H}\right)}. \tag{10}$$

Here, S^* is the length of recirculation cavity in the wake of an isolated building, L is the streamwise length of the upwind building in the lateral direction and W is the width of the building in the crosswind direction. If $S < S^*$, then a street canyon vortex flow parameterization is implemented, otherwise the building is assumed to be isolated and cavity and wake algorithms are utilized [34].

4.1 Modified Röckle model evaluation—7×11 array

In this section, the performance of the MR model is evaluated both qualitatively by comparing general flow features and quantitatively through point-by-point mean velocity comparisons. Our write-up focuses on specific regions of the flow field beginning with the region just upwind of the first row of the 7×11 cube array, followed by the rooftop zone, and ending with the flow in the first street canyon. We begin by looking at the overall flow patterns around the first two rows of buildings.

4.1.1 General comparison of the mean flow field

Figure 7a shows a velocity vector comparison between the experimental data and the MR model in the vertical plane along the centerline at the beginning of the building array. Similar to the case of the SR model, the MR model does a reasonably good job of predicting the location of the stagnation point on the upwind face of the first-row building ($z/H \sim 0.7$). Upwind of the first building, the MR upwind cavity algorithm significantly improved the results by

producing a smaller recirculation cavity, which is in agreement with the experimental data. The plan view in Fig. 7b illustrates the flow structure improvement of the MR model over the SR model (Fig. 5b). The MR scheme agrees well with the strength and direction of the winds that were measured on the front side near ground level at $z/H = 0.2$. The SR scheme (Fig. 5b), however, shows an overly large region of near-zero winds upwind of the building that disagrees with the measurements.

While the experimental data do not show the recirculation region expected along the rooftop of the first building (possibly do to a lack of spatial resolution of the measurements), the velocities decay substantially and show vertical velocity components. As compared to the SR model (Fig. 5a), the MR model (Fig. 7a) improves the results by producing a rooftop recirculation zone and more realistic updrafts and downdrafts. Figure 7a shows that the rooftop recirculation scheme is correctly turned off on row 2 (and beyond) through logic integrated into the MR model.

As compared with the SR model (Fig. 5a), the SC vortex computed by the MR model (Fig. 7a) matches the wind-tunnel data better by reducing the SC vortex strength. The MR street canyon model predicts the center of the vortex to be slightly closer to the experimental data due to the wedge scheme that mimics diffusion of winds from aloft, although it is still shifted to the right compared to the data. Both the SR as well as the MR schemes produce winds that revert to purely horizontal flow too quickly, while the measurements show a significant downward component at the midpoint of the canyon. Figures 5c and 7c depict the wind patterns in the first canyon near ground level at $z/H = 0.2$. Both the SR and MR schemes generate counter-rotating vortices in agreement with the measurements. As compared to the SR scheme (Fig. 5c), the MR scheme (Fig. 7c) matches the strength of the wind and the vortex location better, in part due to the lateral diffusion wedges and the lateral velocity gradient described above.

4.1.2 Upstream flow field

Figure 8 shows a velocity profile comparison of the normalized (a) streamwise and (b) vertical velocities upstream of the building along the centerline of the domain. The streamwise and vertical velocity measurements show that the upwind recirculation zone starts at about $x/H \sim -0.5$. As shown in the Fig. 7 vector plot, the MR model predicts the upwind extent to be $x/H \sim -0.7$. It is clear from Fig. 8 that the upwind cavity zone computed by the SR model is apparent much further upstream ($x/H = -1.0$), where near zero velocities are found between the ground and $z/H \sim 0.25$. At this upwind distance, both the experimental data and the MR model show a logarithmic behavior in the streamwise velocity.

At $x/H = -0.5$, the SR model predicts a near-zero streamwise velocity between the ground and $z/H \sim 0.5$ (Fig. 8a). The experimental data and the MR model, however, continue to show a positive velocity gradient in this region, although the MR model shows more reduction in wind speed compared to the measurements. Above $z/H \sim 0.5$, the experimental data, the SR model and the MR model are all in agreement. At $x/H = -0.25$ and -0.1, the SR model continues to produce near-zero streamwise velocities below $z/H = 0.6$. In contrast, the experimental data and the MR model show reverse flow near the ground. At $x/H = -0.1$, significant reverse flow is still not apparent near the ground in the SR model results. It is interesting to note that at this distance the MR model has a smoother transition into the boundary-layer flow above the building height, likely due to upstream propagation of the effect of the rooftop recirculation found in the MR model. Unphysical kinks in both the SR and MR model-produced streamwise velocity profiles at $x/H = -0.1$ and -0.5 are

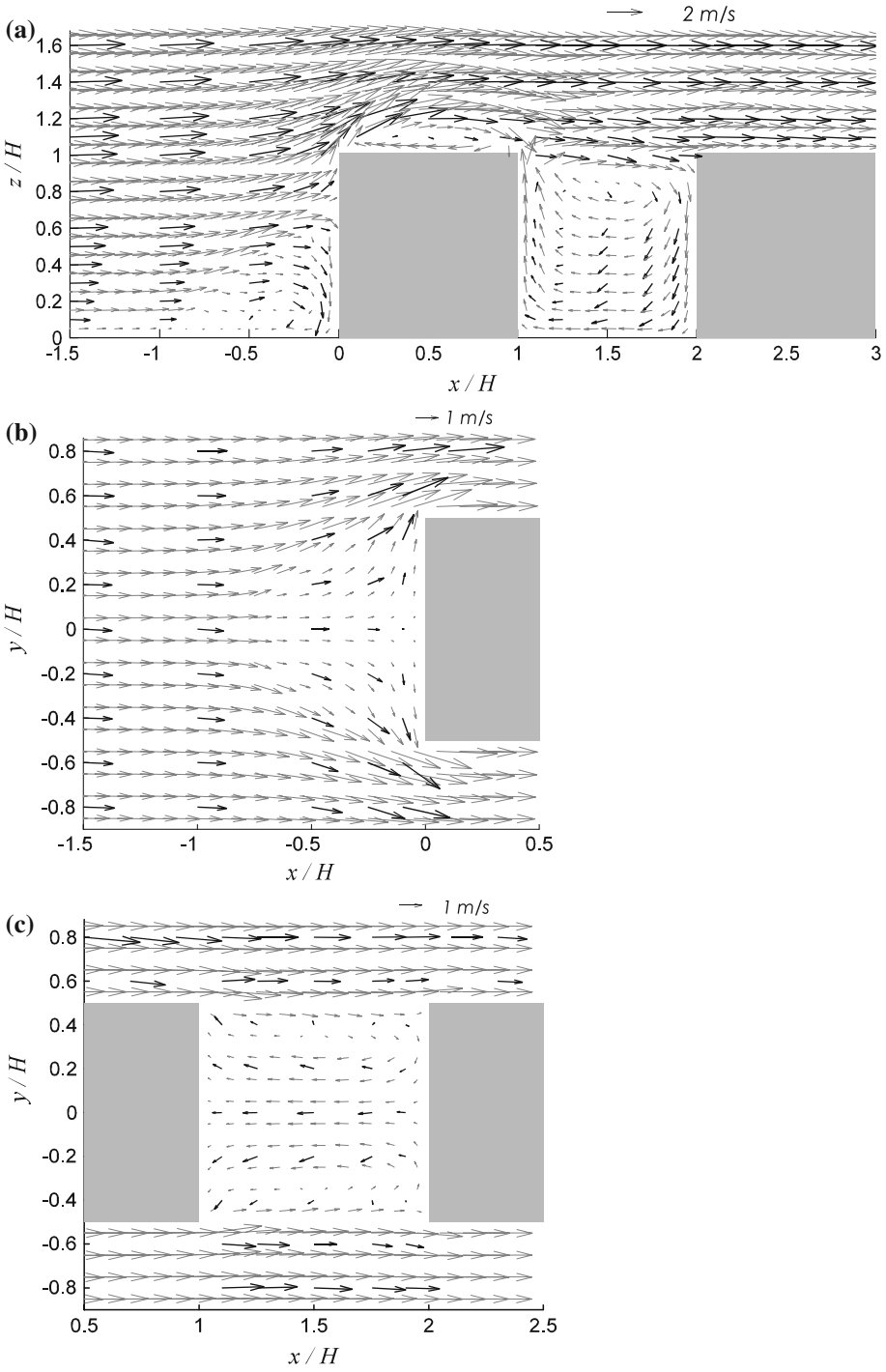

Fig. 7 Comparison of the MR model-computed velocity vectors (gray) with the experimental measurements (black) (**a**) in the x–z plane along the building centerline, (**b**) in the x–y plane at $z/H = 0.2$ upwind of the central building in the first row and (**c**) in the x–y plane at $z/H = 0.2$ in the first row street canyon

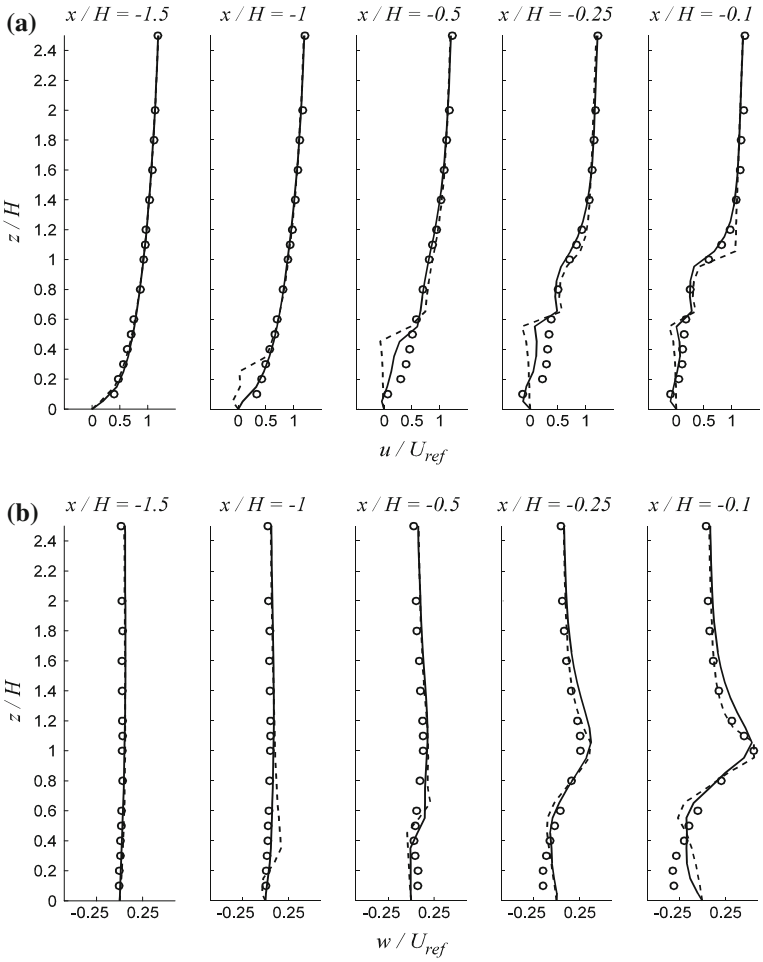

Fig. 8 Centerline profiles of (**a**) streamwise and (**b**) vertical velocities at five streamwise locations *upstream* of the building—experimental data (open circles), SR (dashed line) and MR (solid line)

found at the transition between the upwind cavity zone and ambient flow due to a lack of momentum diffusion in Röckle-style models.

The upstream vertical velocity profiles in Fig. 8b at $x/H = -1$ demonstrate that the SR model slightly overestimates the vertical velocity from $0.3 < z/H < 1$, whereas the MR model and the experimental data are near-zero and in much better agreement. A small kink in the vertical velocity profiles (also seen in the u velocity in Fig. 8a) is observed in both the SR and MR model near $z/H \sim 0.6$ at $x/H = -0.5$ as a result of insufficient model diffusion between the interface of the recirculation zone and the boundary layer. Both the SR and MR models underestimate the magnitude of the vertical velocities near the ground at $x/H = -0.25$ and -0.1, but both models are in general agreement with the experimental results above the stagnation point location, where a strong updraft is observed.

Table 1 summarizes the RMS error difference between the MR and SR models for the available experimental data upwind of the first building. The average error in the MR model is approximately 60% of the SR model.

Table 1 Cumulative average RMS error for the two models compared to the 7×11 experimental data

	Upstream	Rooftop	Street canyon	Total
% Error (RMS)				
Standard Röckle	10.4	13.7	20.2	17.2
Modified Röckle	6.1	7.2	9.5	8.4

4.1.3 Rooftop flow field

Figure 9 shows model-produced and measured vertical profiles of the normalized (a) streamwise and (b) vertical velocities at the rooftop of the first building along the centerline of the domain. As the upwind flow strikes the front building, the flow separates from the rooftop. The separated flow reattaches near the end of the rooftop forming a recirculation region. As noted earlier, the SR model does not simulate a recirculation region on the rooftop. Hence, the streamwise velocity profile in Fig. 9a confirms that the SR model overestimates the streamwise velocities above the rooftop, while MR model produces better agreement with the experimental data for the u velocity at all streamwise locations due to the rooftop recirculation algorithm. At $x/H = 0.3$, 0.5 and 0.7, the MR model shows a slight increase in the streamwise velocity at about $0.25H$ above the rooftop ($z/H = 1.25$) compared to the SR model, but there is not enough experimental data to corroborate this feature. Further downstream ($x/H = 0.7$ and 0.9) just above the rooftop ($z/H = 1.1$), the MR model over predicts the strength of the recirculation. It is interesting to note that at this resolution, the experimental data do not actually show any reverse flow.

Vertical velocities along the rooftop are shown in Fig. 9b. The SR model underestimates the vertical velocities (updraft strength) above the rooftop at $x/H = 0.1$ and 0.3, whereas the experimental data and the MR model are in fair agreement. At $x/H = 0.5$, 0.7 and 0.9 the SR model predicts slightly positive vertical velocities, while the data show a downdraft. The MR model produces a very small slightly positive vertical velocity at $x/H = 0.5$, while the measurements show a very small negative velocity near the rooftop. The MR scheme predicts the vertically velocity very well at $x/H = 0.7$, but over predicts the strength of the downdraft at the end of the building ($x/H = 0.9$).

Figure 10 shows a comparison of vertical profiles of normalized streamwise velocity above the rooftop of the second building along the centerline of the domain. Due to the shielding effect and advection from the rooftop of the first building, the flow striking the second building does not form a recirculation region above the rooftop. The flow forms a wall-normal logarithmic layer on the rooftop of the second building. The streamwise velocity comparison in Fig. 10 shows that the SR model slightly overestimates the velocities above the rooftop, while the MR model generates velocities that agree better with the experimental data. As shown in Table 1, the average RMS error of the MR model is roughly half that of the SR model for the available profiles.

4.1.4 Street canyon flow field

Figure 11 shows a comparison of vertical profiles of normalized (a) streamwise and (b) vertical velocities in the first SC along the centerline of the domain. As demonstrated earlier in Fig. 5a, our implementation of the SR model produces a SC vortex with an elevated core, a region of streamwise flow above the vortex core that is too small, and a region of backflow below the vortex core that is too large compared to the measurements. As shown in Fig. 11a,

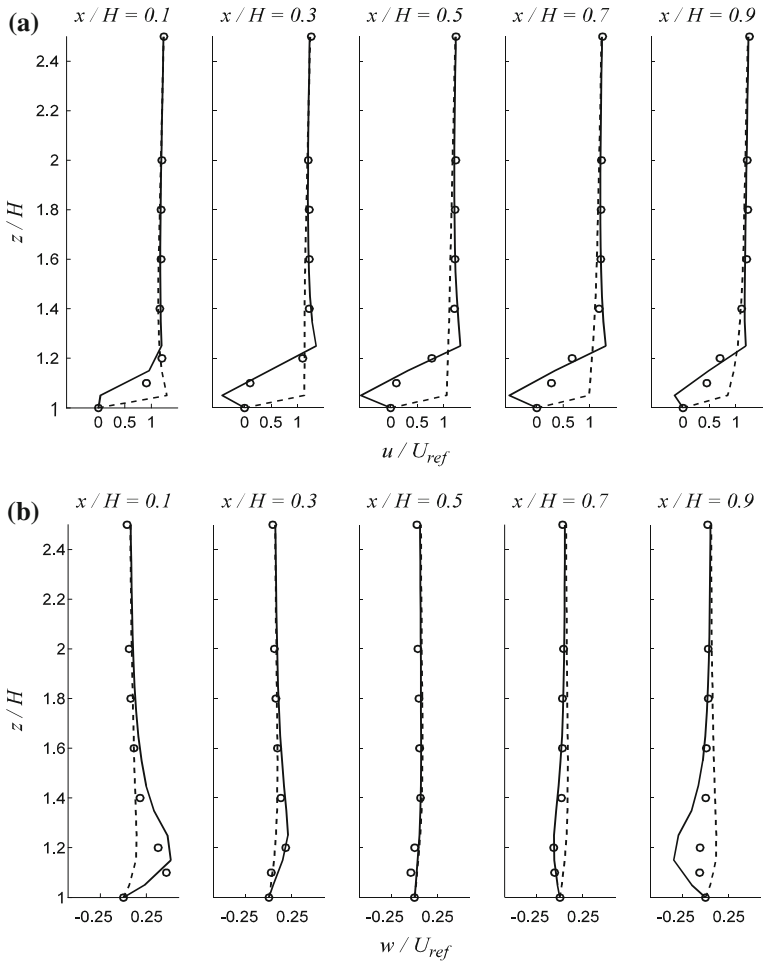

Fig. 9 Centerline profiles of (**a**) streamwise and (**b**) vertical velocities at five streamwise locations on the *rooftop* of the *first building*—experimental data (open circles), SR (dashed line) and MR (solid line)

the SR model is in reasonably good agreement with the experimentally measured streamwise velocity within the SC below $z/H \sim 0.6$ at all locations, although at $x/H = 1.25$ and 1.5, the SR model slightly overestimates the magnitude of backflow in the canyon. Near $z/H \sim 1$, the SR model results in a strong shear in streamwise velocity due to the lack of downward diffusion of streamwise momentum from aloft. The MR model is in excellent agreement with the streamwise velocity data in the canyon and is in better agreement than the SR model near the building height ($z/H \sim 1$). The streamwise velocities calculated using the MR model yield a smoother transition from the canyon flow to the boundary-layer flow aloft due to the incorporation of the wedge diffusion parameterization.

The vertical profiles of the vertical velocities shown in Fig. 11b at $x/H = 1.1$ and 1.25 indicate that both models overestimate the vertical velocities, although the MR model performs better in the vicinity of the canyon top. Near $z/H \sim 1$, both models give rise to vertical velocities of opposite sign compared to the experimental data. This is a result of an over prediction of the height of the center of the canyon vortex as illustrated in the vector

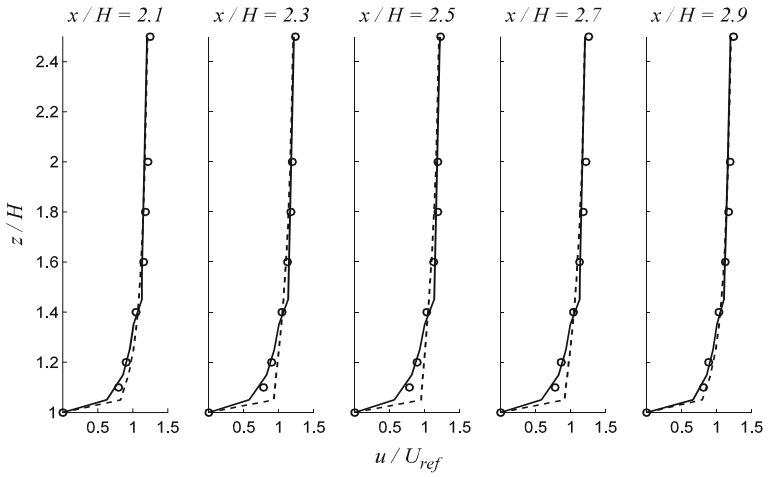

Fig. 10 Centerline profiles of streamwise velocities at five streamwise locations on the *rooftop* of the *second building*—experimental data (open circles), SR (dashed line) and MR (solid line)

plots in Figs. 5 and 7. At $x/H = 1.5$, the SR and MR models generate near zero w velocities as opposed to the negative velocities obtained in the experiment. This is a result of the models predicting a more symmetric vortex about the canyon center, while the experimental data indicate the center of the vortex is shifted slightly upstream. Both the SR and MR models overestimate the w velocity within the canyon at $x/H = 1.75$ and 1.9. A significant improvement is seen in the results of the MR model at $x/H = 1.75$ and 1.9 compared to the SR model, where the w velocity follows the experimental results more closely between $z/H \sim 0.6$ and $z/H \sim 1.6$.

Figures 5c, 7c and 12–15 show velocity vector and profile plots within and just outside of the first street canyon for three different horizontal planes above the ground ($z/H = 0.2$, 0.5 and 0.8). Figures 5c and 7c show the plan view of the model-computed and measured velocity vectors at $z/H = 0.2$ for the SR and MR models respectively. The SR model's SC parameterization significantly overestimates the magnitude of the backflow in the SC near the ground (Fig. 5c). This result stems partly from the strong lateral flux of momentum into the street canyon from the street intersection ($|y|/H > 1$) and partly from the lack of a laterally-varying velocity reduction factor in the SR model. The SC parameterization in the MR model accounts for the advection and diffusion from the intersections as well as from above the SC; this shifts the center of the vortices well inside the SC (see Fig. 7c). The MR model shows a significant improvement in simulating the strength and direction of the mean flow measured in the canyon.

Figure 12 shows a comparison of lateral velocity profiles of normalized (a) streamwise and (b) crosswind velocities in the first SC at $z/H = 0.2$. As shown in Fig. 12a, the SR model creates a strong streamwise velocity gradient near the sides of the SC, while the lateral diffusion associated with the MR model produces a smoother profile that is in better agreement with the experimental data in the interior of the canyon and outwards into the intersection ($|y|/H > 0.5$). The SR model slightly underestimates the streamwise velocities near the center of the canyon at $x/H = 1.25$ and 1.5, while at $x/H = 1.1$, 1.75 and 1.9 the SR model is in agreement with the experimental data. However, the curvature of the SR velocity profile is opposite to the MR model and the experimental data in the canyon.

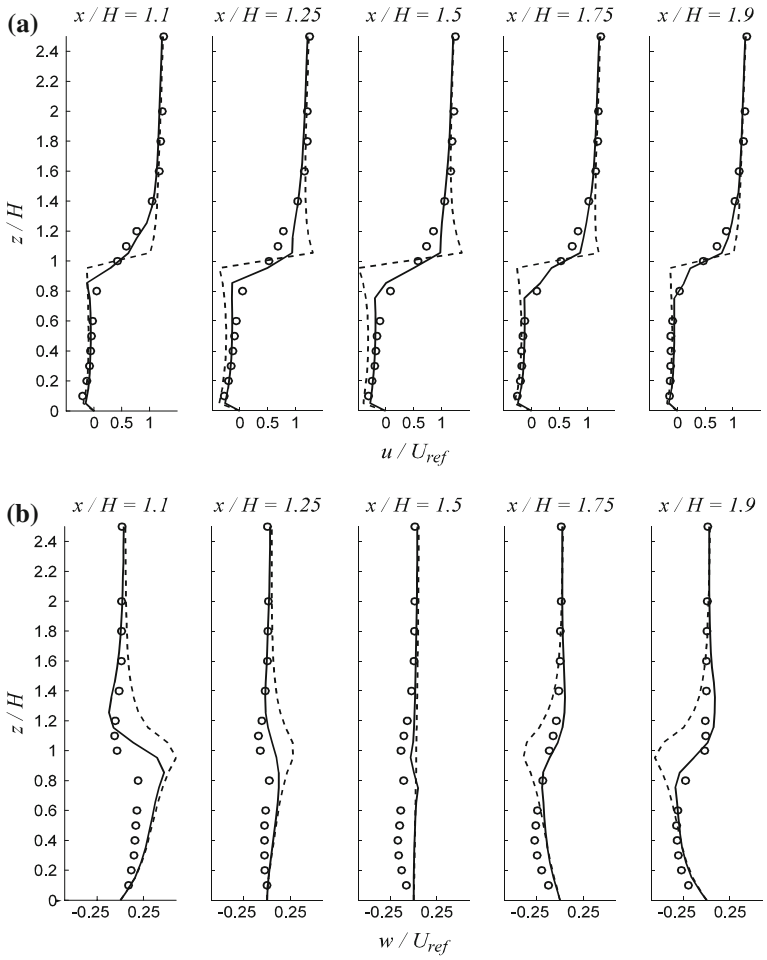

Fig. 11 Centerline profiles of (**a**) streamwise and (**b**) vertical velocities at five streamwise locations in the *first street canyon*—experimental data (open circles), SR (dashed line) and MR (solid line)

The crosswind velocity profiles in Fig. 12b show that the MR model captures the lateral flow better than the SR model at $z/H = 0.2$. As explained earlier, the SR model significantly overestimates the magnitude of the crosswind velocity from $0.2 < |y|/H < 0.8$ at $x/H = 1.1$ and 1.25. Downstream of the canyon center, an opposite trend in the crosswind velocity profile is observed in the SR model at $x/H = 1.75$ and 1.9. The SR model agrees with the experimental data in the interior of the canyon ($|y|/H < 0.2$) at $x/H = 1.1$ and 1.25. The magnitude of the lateral velocity computed by the MR model is in better agreement with the measurements at all the streamwise locations, but of opposite sign from $1.1 < x/H < 1.75$.

Figures 13 and 14 show plan view comparisons of the velocity vectors at $z/H = 0.5$ and $z/H = 0.8$, respectively, from the (a) SR and (b) MR models with the experimental data. The plots clearly illustrate the behavior of the wall normal vortices formed in the SC. Similar to the $z/H = 0.2$ case, the SR model significantly over predicts the magnitude of the velocities within the SC and poorly predicts both the streamwise and lateral locations of the center of the wall normal vortices. Again, due to the lack of lateral diffusion into the street

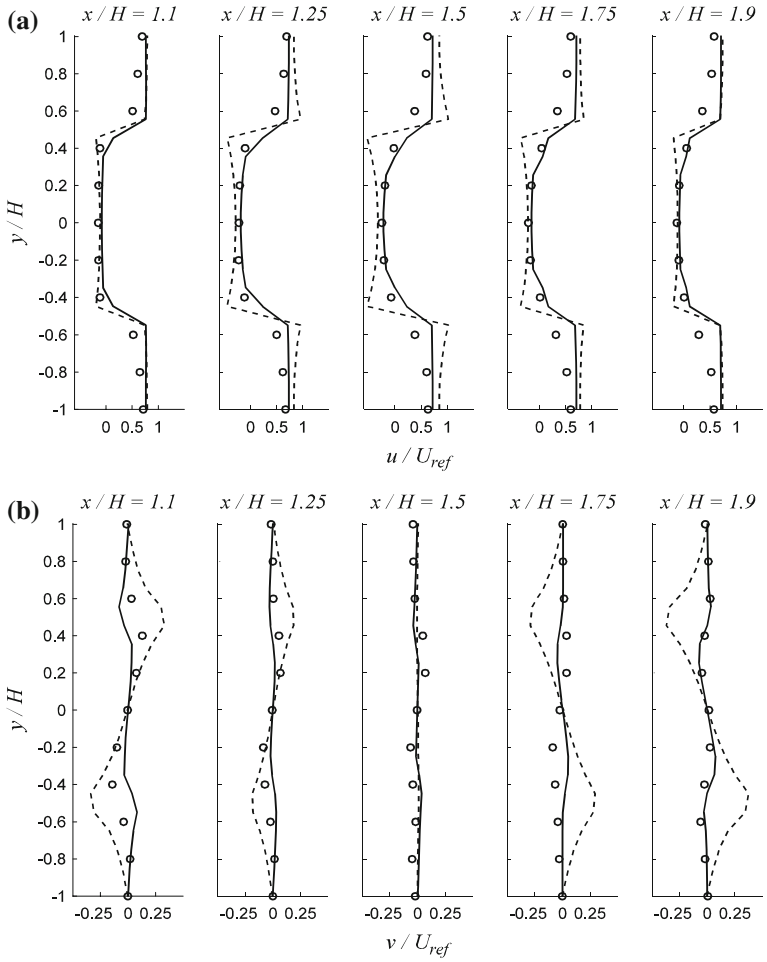

Fig. 12 Lateral profiles of the (**a**) streamwise and (**b**) crosswind velocities at five streamwise locations at $z/H = 0.2$ in the *first street canyon*—experimental data (open circles), SR (dashed line) and MR (solid line)

canyon associated with the SR model, the simulated velocity vectors near the end of the SC do not match the experimental results in direction or magnitude. The MR model, however, significantly improves the direction as well as magnitude of velocity vectors at the lateral ends of the SC compared to SR simulation. The downstream centers of the lateral vortices in the experimental data show a systematic shift upstream with height above the canyon floor. This behavior is similar to the "rainbow vortex" identified in the wake of an isolated cube by Hunt et al. [30]. This phenomena, which is associated with the change in flow direction near $x/H = 1.5$ (in the $z/H = 0.8$ slice), is a result of downward diffusion of momentum that is better captured in the MR model than in the SR model.

Figure 15 shows a comparison of the lateral velocity profiles of the normalized streamwise velocities in the first SC at (a) $z/H = 0.5$ and (b) $z/H = 0.8$. The comparison of the models with the experimental data is quite similar to the descriptions given above for $z/H = 0.2$ with overly strong shear at the lateral edges of the canyon and incorrect prediction of the curvature of the velocity profile. However, the under estimation of the u velocity by the SR model within the SC becomes much more pronounced higher up in the canyon and further

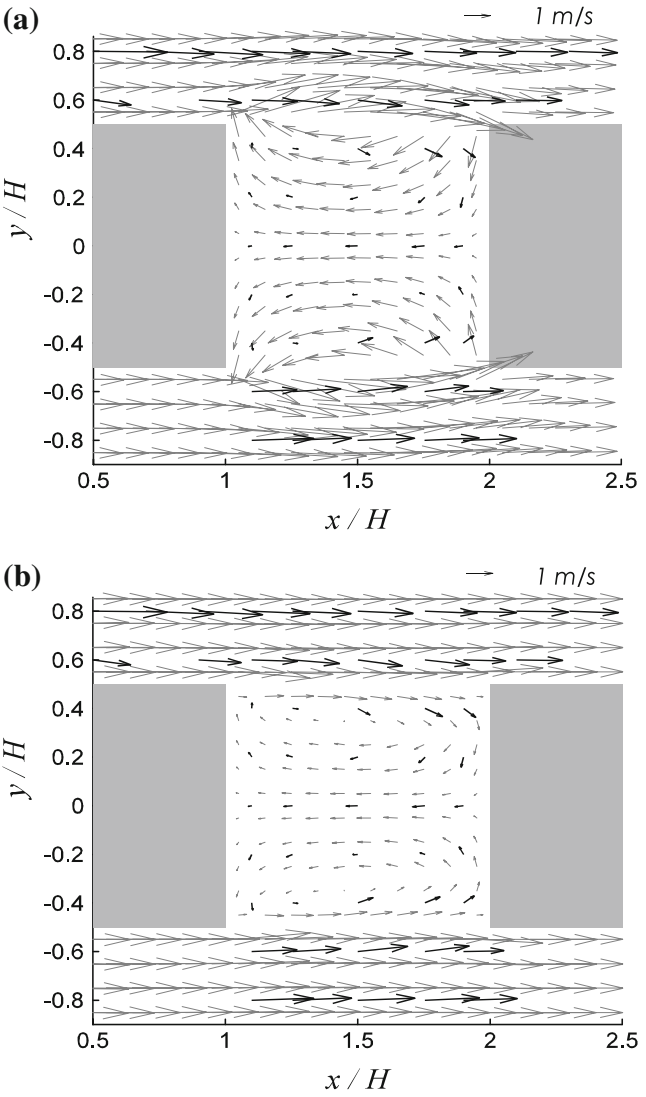

Fig. 13 Plan view velocity vector comparison of (**a**) the SR and (**b**) MR models (gray) with the experimental data (black) at $z/H = 0.5$ in the *first street canyon*

downstream, while the MR model agrees quite well with the experimental data. As shown in Table 1, the average RMS error in the SC for the MR model is slightly less than half that of the SR model for the available profiles.

4.2 Wide building test case

4.2.1 Wind-tunnel experiment

As a second evaluation test case, a wide building street canyon experimental data set was utilized. The data were obtained by researchers in the Institute of Hydromechanics at Uni-

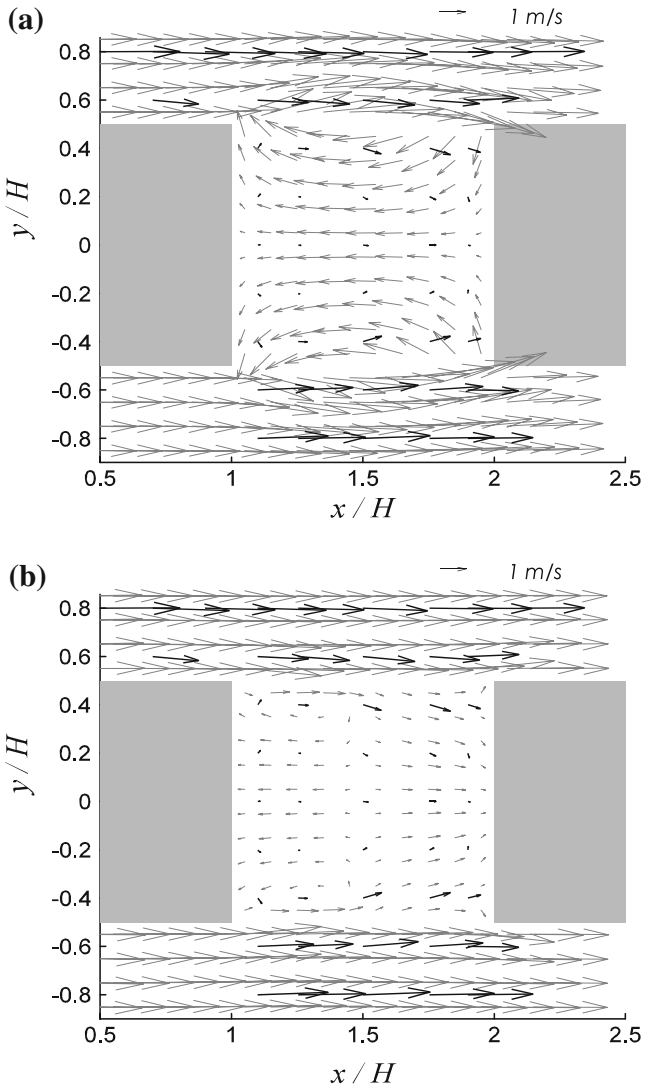

Fig. 14 Plan view velocity vector comparison of (**a**) the SR and (**b**) MR models (gray) with the experimental data (black) at $z/H = 0.8$ in the *first street canyon*

versity of Karlsruhe (for details, see [35,36]). The researchers used a 2 m wide by 1 m high test section in a neutrally stratified atmospheric boundary layer wind tunnel. Two building rows were mounted on the floor of the test section surrounded by homogenously distributed roughness elements. The street canyon was oriented normal to the incident wind. The buildings were wide with widths ten times the building height (i.e., $W = 10H$; $H = L$), and the distance between the buildings was $S = H$ (see Fig. 16). The boundary layer flow was generated by employing vortex generators at the tunnel entrance and roughness elements on the floor. According to Kastner-Klein and Plate [36], the inlet mean velocity profile can be described by a power law with an exponent of 0.23. The Reynolds number for this flow was

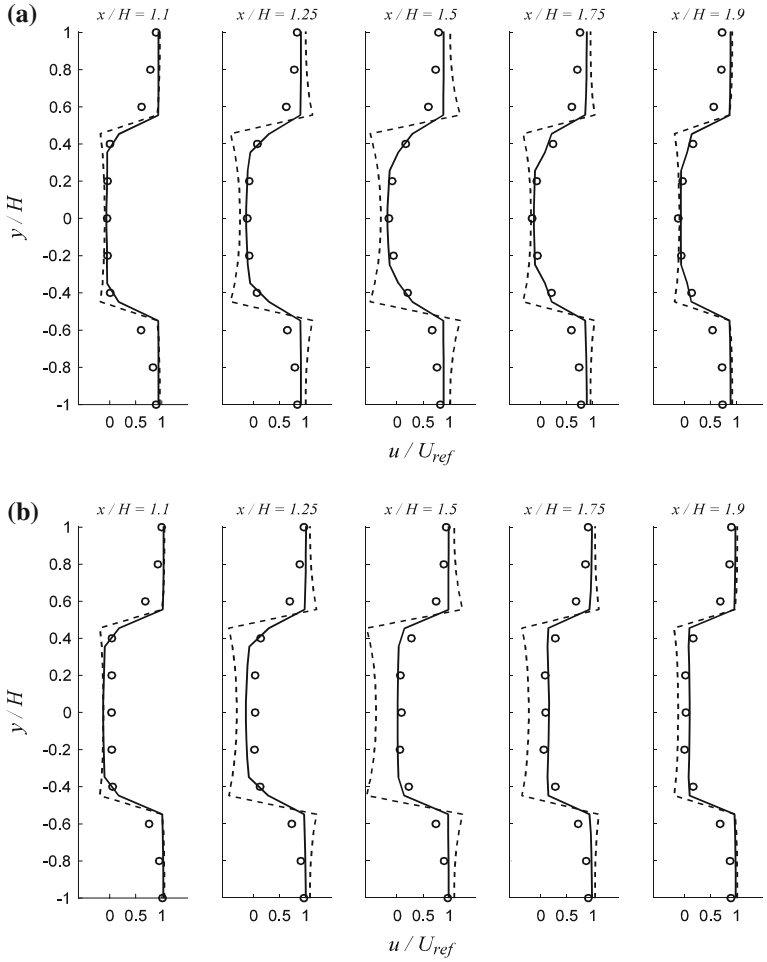

Fig. 15 Lateral profiles of the streamwise velocity at five streamwise locations at (**a**) $z/H = 0.5$ and (**b**) $z/H = 0.8$ in the *first street canyon*—experimental data (open circles), SR (dashed line) and MR (solid line)

approximately 56,000 with a reference velocity of 7 ms^{-1} at a reference height (H) of 0.12 m. The measurements were taken using Laser-Doppler velocimetry (LDV) and a single hotwire.

4.2.2 Description of the test case

Following Kastner-Klein and Plate [36], a power law profile with an exponent of 0.23 was specified as the inlet velocity profile for running the SR and MR models. Similar to the 7×11 building array test case, the velocity boundary conditions at the inlet, outlet and along the top of the domain were Dirchlet and specified by the initial power law profile. The simulations were run with a grid resolution 0.012 m such that the buildings were resolved with 10 cells in each direction. The domain size used for the simulations was $0.960\,\mathrm{m} \times 1.680\,\mathrm{m} \times 0.240\,\mathrm{m}$ ($80 \times 140 \times 20$ in grid cell units).

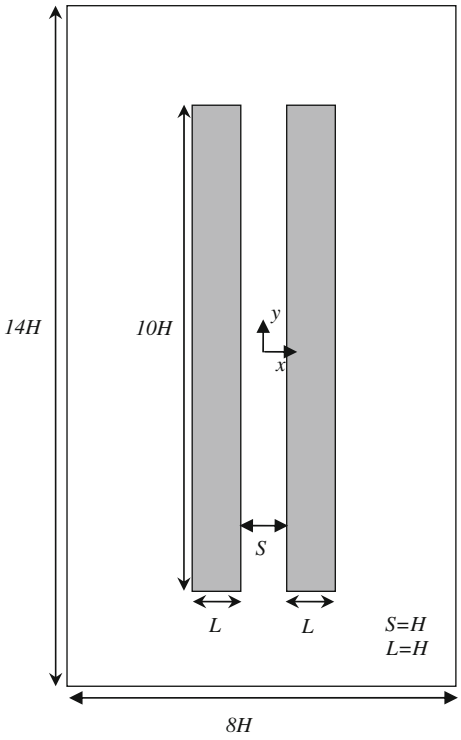

Fig. 16 Schematic of the wide building street canyon computational domain used in the QUIC-URB simulations

4.2.3 Model-measurement comparison

Unfortunately, this wide building data set did not include measurements immediately upstream or along the rooftop of the buildings, hence this section only discusses the comparison between the results obtained from the SR model, MR model and the wind-tunnel experiment in the street canyon region between the two wide buildings.

Figure 17 shows a velocity vector comparison between the experimental data, the (a) SR and (b) MR models in the vertical plane along the centerline of the domain. Like the 7×11 array test case, the SR model produces stronger downdrafts and backflow as compared to the experimental data for the wide building case. The center of the SC vortex computed using the SR model is raised well above the height of the vortex center indicated by the experimental data. The MR model predicts the center of the vortex to be slightly closer to the experimental data due to the wedge scheme that mimics the diffusion of winds from aloft, although it is still higher than the experimental data.

Figure 18 shows a comparison of vertical profiles of normalized (a) streamwise and (b) vertical velocities in the SC along the centerline of the domain. As in the 7×11 test case, the SR model produces a SC vortex with an elevated core and a region of streamwise flow above the vortex core that does not penetrate far enough down into the canyon. As shown in Fig. 18a, the SR model is in reasonably good agreement with the experimentally-measured streamwise velocity within the SC below $z/H \sim 0.6$ at all locations. Near $z/H \sim 1$, the SR model produces large streamwise velocity gradients due to the lack of downward diffusion of streamwise momentum from aloft. Similar to the SR model, the MR model is in agreement with the streamwise velocity data within the canyon. The MR model, however, is in better

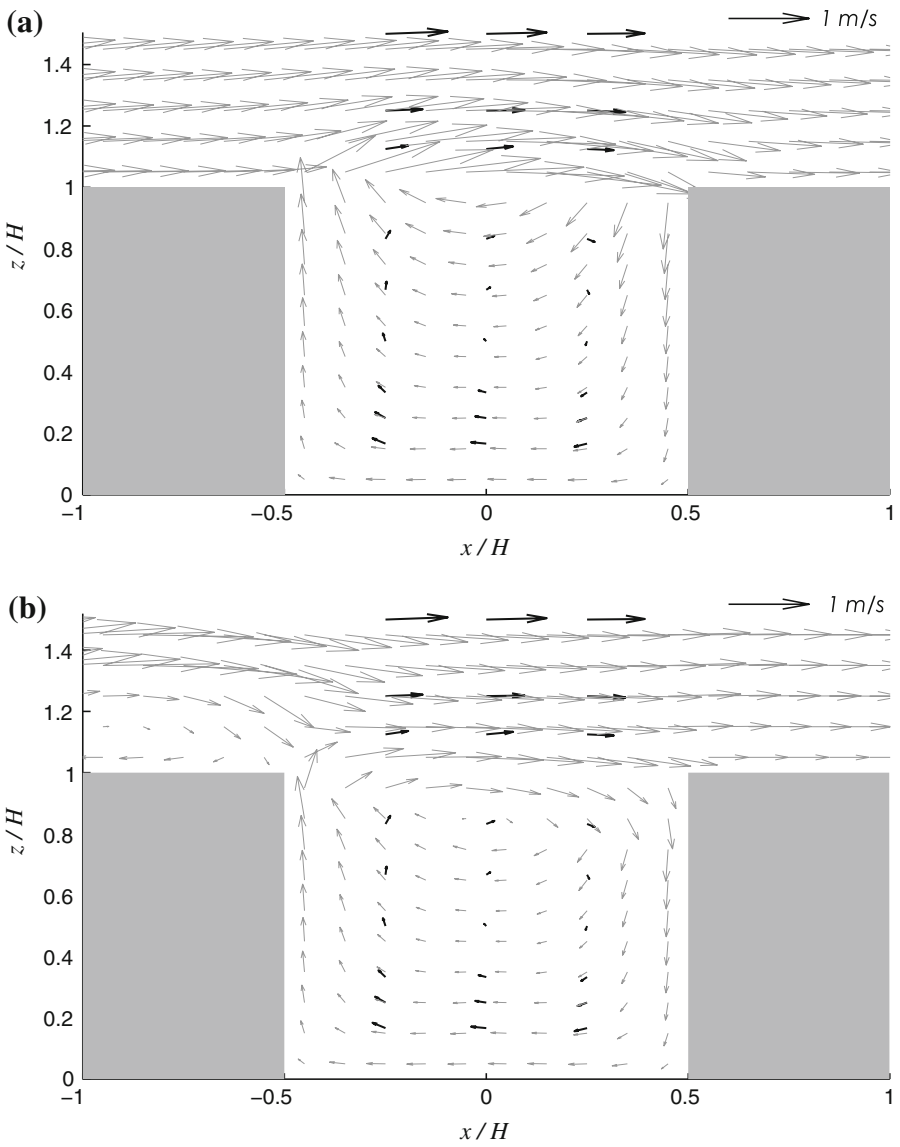

Fig. 17 Centerline velocity vector comparison of (**a**) the SR and (**b**) MR models (gray) with the experimental data (black)

agreement than the SR model near the building height ($z/H \sim 1$). The MR model yields a smoother transition of streamwise velocities from the canyon to the boundary-layer flow aloft due to the incorporation of the wedge diffusion parameterization.

The vertical profiles of the vertical velocities shown in Fig. 18b at $x = -0.25$ indicate that both models slightly underestimate the vertical velocities below $z/H \sim 0.4$. The MR model performs slightly better than the SR model from $0.6 < z/H < 1.4$. In addition, the SR model over predicts the updraft close to the height of the building ($z/H \sim 1.0$). At

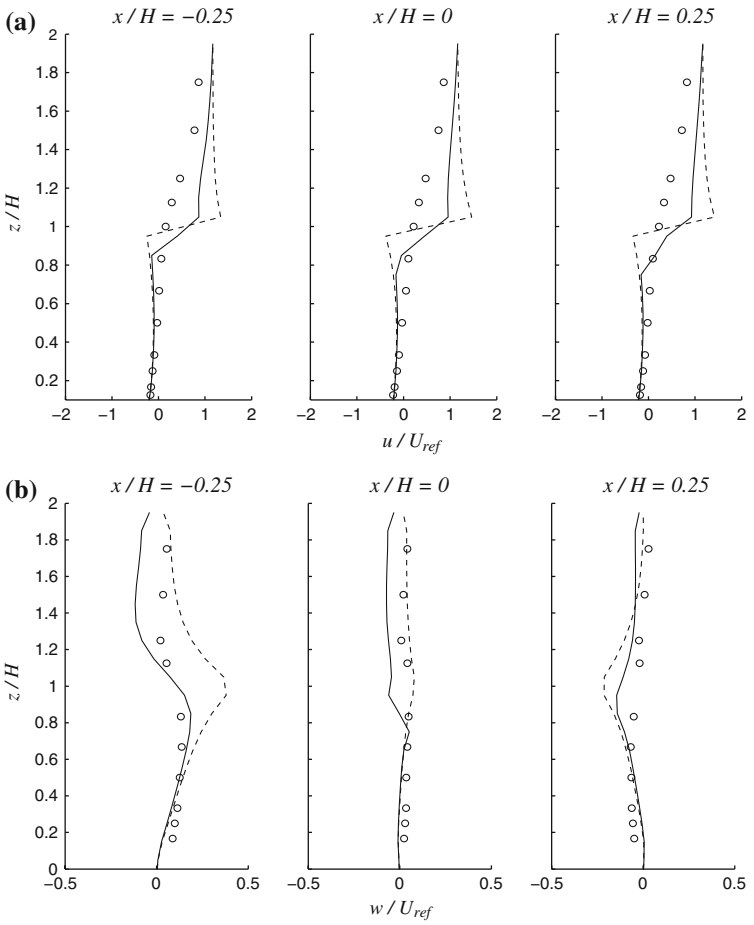

Fig. 18 Centerline profiles of (**a**) streamwise and (**b**) vertical velocities at three streamwise locations in the *wide street canyon*—experimental data (open circles), SR (dashed line) and MR (solid line)

$x/H = 0$, both the models underestimate the vertical velocity within the canyon yielding similar results, however the SR model performs better than the MR model above the street canyon region. This is likely the result of an overly intense rooftop recirculation region on the upwind building. At $x/H = 0.25$, both models slightly overestimate the vertical velocities below $z/H \sim 0.4$. The MR model performs better than the SR model from $0.6 < z/H < 1.4$, where the SR model over predicts the downdraft velocities.

Figure 19 shows a comparison of lateral profiles of normalized streamwise velocities over half of the SC at $z/H = 0.25$. As shown in Fig. 19, the SR model creates a strong streamwise velocity gradient near the sides of the SC due to the absence of lateral diffusion, while the MR model produces a smoother profile that is in better agreement with the experimental data at the sides of the canyon ($y/H \sim -5.0$). Both models are in agreement with the experimental data within the SC, however they overestimate the streamwise velocity outside of the canyon ($y/H < -5.0$). The MR model performs slightly better than the SR model outside of the canyon. Similar to the 7×11 array case, the curvature of the SR velocity profile is opposite to the MR model and the experimental data in the canyon. As summarized in Table 2, the RMS error of the MR model is about ~30% less than the error associated with the SR model.

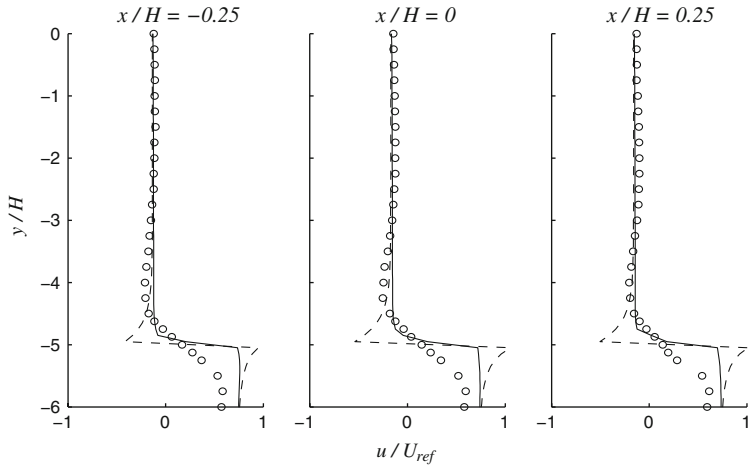

Fig. 19 Lateral velocity profiles of streamwise velocities at three streamwise locations in the *wide street canyon*-experimental data (open circles), SR (dashed line) and MR (solid line)

While this is not quite as good as the results from the 7×11 array, it represents a substantial improvement.

5 Conclusions

Transport and dispersion in urban environments is extremely complicated. Buildings alter the flow fields and deflect the wind, causing updrafts and downdrafts, channeling between buildings, areas of calm winds adjacent to strong winds, and horizontally and vertically rotating-eddies between buildings, at street corners, and other places within the urban canopy (see review by Hosker [29]). This makes it very difficult to devise fast response urban dispersion models that will work at the street canyon to neighborhood scales.

Röckle [48] developed a methodology for quickly computing 3D wind fields around buildings using an empirical-diagnostic approach. The Röckle modeling strategy is a unique and potentially powerful tool because it rapidly produces spatially-resolved wind fields in urban areas that can be used to drive urban dispersion models. Röckle-type models do not solve transport equations for momentum or energy; rather, they rely heavily on empirical parameterizations and mass conservation. In this paper, we evaluate a fast-running wind model that is based on the Röckle formulism called QUIC-URB using wind measurements from two wind tunnel data sets: an idealized 7×11 cubical building array and a wide building street canyon. In the model-experiment comparison, we test two empirical building flow parameterizations within the QUIC-URB model: the standard Röckle (SR) algorithms and the modified Röckle (MR) algorithms.

To our knowledge, this is the most rigorous comparison of a Röckle-type wind model in the literature. The results indicate that our implementation of the SR model produces wind fields that are in reasonable agreement with experimental data within the urban street canyon, however the velocities are generally too strong and the location of vortex centers in various planes are shifted toward the edges of the street canyon where the wind shear is highest. Upstream of the first building, the SR model produces a recirculation cavity that is larger

Table 2 Cumulative average RMS error for the two models compared to the wide building experimental data

	Street canyon
% Error (RMS)	
Standard Röckle	23.9
Modified Röckle	16.9

than experimentally expected and poorly predicts the velocities in this region. Above the buildings along the rooftop, the SR does not account for the potential of rooftop recirculation.

The MR model attempts to build on the strengths of the SR model and introduces additional physically-based, but simple parameterizations that significantly improve the results in most regions of the flow in the 7×11 array and wide street canyon. The MR model produces vortices within street canyons that have velocities that compare much more favorably to the experimental results with the vortices shifted inward away from the edges of the street canyon. This is largely accomplished by modeling the effect of advection and momentum diffusion from outside the street canyon into the street canyon on the sides and from aloft. Upstream of the first building, a reduced velocity displacement zone and simple trigonometric vortex parameterization produce greatly improved results. Above the first rooftop, the rooftop recirculation zone improves the results. In addition, logic that removes the recirculation zone from downstream buildings produces physically realistic results in groups of buildings.

We expect that these improvements in the wind field will result in improved dispersion calculations in built environments. A future paper will include dispersion comparisons using the QUIC-Plume Lagrangian dispersion model in the same 7×11 array. As a final note, we stress the importance of testing multi-building parameterizations under a wide range of non-idealized conditions. Since it is quite rare that buildings in real cities take on the form that the original parameterization were developed from, the model may not yield physically reasonable results when generalized. Hence, it is imperative to rigorously evaluate the model for a wide range of scenarios. This is one of the greatest challenges in utilizing Röckle type wind models.

Acknowledgements This work has been supported by the Biological Countermeasures Office in the Department of Homeland Security and by the Joint Science Technology Office in the Defense Threat Reduction Agency.

References

1. Allwine KJ, Shinn JH, Streit GE, Clawson KL, Brown MJ (2002) Overview of URBAN 2000: a multiscale field study of dispersion through an urban environment. Bull Am Meteorol Soc 83:521–536. doi:10.1175/1520-0477(2002)083<0521:OOUAMF>2.3.CO;2
2. Allwine KJ, Leach ML, Stockham LW, Shinn JS, Hosker RP, Bowers JF et al (2004) Overview of joint urban 2003—an atmospheric dispersion study in Oklahoma city. Preprints. In: Symposium on planning, nowcasting, and forecasting in the urban zone, Seattle, WA, Am Meteorol Soc, CDROM J7.1
3. Bagal N (2005) Development and testing of empirical parameterizations for the quick urban and industrial complex model. Masters Thesis, University of Utah
4. Bagal N, Pardyjak ER, Singh B, Brown MJ (2004) Implementation of rooftop recirculation parameterization in the QUIC fast response urban wind model. Preprints. In: Fifth AMS symposium urban environment, Vancouver, BC, Am Meteorol Soc, CDROM 6.10
5. Bagal N, Pardyjak ER, Brown MJ (2004) Improved upwind cavity parameterization for a fast response urban wind model. Preprints. In: Symposium on planning, nowcasting, and forecasting in the urban zone, Seattle, WA, Am Meteorol Soc, CDROM P1.13

6. Belcher SE (2005) Mixing and transport in urban areas. Philos Trans R Soc A 363:2947–2968. doi:10.1098/rsta.2005.1673
7. Berkowicz R (2000) OSPM—a parameterized street pollution model. Environ Monit Assess 65:323–331. doi:10.1023/A:1006448321977
8. Booth TM, Pardyjak ER (2006) Validation of a data assimilation technique for an urban wind model. Preprints. In: Fifth AMS symposium urban environment, Atlanta, GA, Am Meteorol Soc, CDROM J4.9
9. Bradbury L, Castro I (1971) A pulsed-wire technique for velocity measurements in highly turbulent flows. J Fluid Mech 49:657–691. doi:10.1017/S0022112071002313
10. Brook DR, Felton NV, Clem CM, Strickland DCH, Griffiths IH, Kingdon RD et al (2003) Validation of the urban dispersion model (UDM). Int J Environ Pollut 20:11–21
11. Brown M, Lawson R, DeCroix D, Lee R (2001) Comparison of centerline velocity measurements obtained around 2D and 3D building arrays in a wind tunnel. Int Soc Environ Hydraulics, Tempe, AZ, LA-UR-01-4138, 6 pp
12. Castro IP, Robins AG (1975) The effect of a thick incident boundary layer on the flow around a small surface mounted cube. CEBG Laboratory note R/M/N795
13. Chan S, Humphries T, Lee R (2004) A simplified CFD approach for modeling urban dispersion. Preprints. In: Symposium on planning, nowcasting, and forecasting in the urban zone, Seattle, WA, Am Meteorol Soc, CDROM 6.4
14. Coirier WJ, Reich AJ (2003) Oklahoma city high-resolution dispersion simulation. CFDRC report 8520(1)
15. Dabberdt W, Ludwig F, Johnson W (1973) Validation and applications of an urban diffusion model for vehicular pollutants. Atmos Environ 7:603–618. doi:10.1016/0004-6981(73)90019-X
16. DeCroix D, Brown M (2002) Report on CFD model evaluation using URBAN 2000 field experiment data: IOP 10, release 1, 26 October, 2000. LA-UR-02-4755, 80 pp
17. Doran JC, Allwine KJ, Clawson KL, Carter RG (2006) Retention of tracer gas from instantaneous releases of SF6 in an urban environment. In: 14th Joint conference on the applications of air pollution meteorology with the air and waste management association, Atlanta, GA, Am Meteorol Soc, CDROM 6.2
18. Eerens HC, Sliggers CJ, van den Hout KD (1993) The CAR model: the Dutch method to determine city street air quality. Atmos Environ 27B:389–399
19. Fackrell JE (1984) Parameters characterising dispersion in the near wake of buildings. J Wind Eng Ind Aerodyn 16:97–118. doi:10.1016/0167-6105(84)90051-5
20. Genikhovich EL, Snyder WH (1994) A new mathematical model of pollutant dispersion near a building. Preprints. In: 8th AMS/AWMA conference on application of air pollution meteorology, Nashville, TN, pp 254–261
21. Gowardhan AA, Brown MJ, Pardyjak ER (2008) Evaluation of a fast response pressure solver for flow around an isolated cube. Env Fluid Mech (submitted)
22. Gross G (1997) ASMUS-Ein numerisches model zur berechnung der strömung und der schadstoffverteilung im bereich einzelner gebaude. II Schadstoffausbreitung und anwendung. Meteorol Z 6: 130–136
23. Gross G, Röckle R, Janssen U (1994) ASMUS-Ein numerisches model zur berechnung der strömung und der schadstoffverteilung im bereich einzelner gebäude. I Das strömungsfeld. Meteorol Z 3:267–274
24. Hall D, Spanton A, Griffiths I, Hargrave M, Walker S (2000) The UDM: a model for estimating dispersion in urban areas. Technical report no 03/00 (DERA-PTN-DOWN)
25. Hanna SR, Britter R, Franseze P (2003) A baseline urban dispersion model evaluated with Salt Lake City and Los Angeles tracer data. Atmos Environ 37:5069–5082. doi:10.1016/j.atmosenv.2003.08.014
26. Hanna SR, Reynolds RM, Heiser J, Bornstein R (2004) Plans for the Madison Square Garden 2004 (MSG04) tracer experiment in Manhattan. Preprints. In: Fifth AMS symposium urban environment, Vancouver, BC, Am Meteorol Soc, CDROM 1.5
27. Hanna SR, Brown MJ, Camelli FE, Chan ST, Coirier WJ, Hansen OR, Huber AH, Kim S, Reynolds RM (2006) Detailed simulations of atmospheric flow and dispersion in downtown Manhattan. Bull Am Meteorol Soc 87(12):1713–1726
28. Hanna SR, White J, Zhou Y, Kosheleva A (2006) Analysis of JU2003 and MSG05 meteorological and tracer data. Preprints. In: 6th AMS symposium urban environment, Atlanta, GA, CDROM 1.5
29. Hosker RP (1984) Flow and diffusion near obstacles. In: Randerson D (ed) Atomospheric science and power production, publication DOE/TIC-27601. Technical information center, US DOE, pp 241–326
30. Hunt JCR, Abell CJ, Peterka JA, Woo H (1978) Kinematical studies of the flows around free or surface-mounted obstacles; applying topology to flow visualization. J Fluid Mech 86:179–200. doi:10.1017/S0022112078001068
31. Hussain M, Lee BE (1980) A wind tunnel study of the mean pressure forces acting on large groups of low rise buildings. J Wind Eng Ind Aerodyn 6:207–225. doi:10.1016/0167-6105(80)90002-1
32. Irwin H (1981) The design of spires for wind simulation. J Wind Eng Ind Aerodyn 7:361–366 doi:10.1016/0167-6105(81)90058-1

33. Jackson PS (1981) On the displacement height in the logarithmic velocity profile. J Fluid Mech 111: 15–25
34. Kaplan H, Dinar N (1996) A Lagrangian dispersion model for calculating concentration distribution within a built-up domain. Atmos Environ 30:4197–4207. doi:10.1016/1352-2310(96)00144-6
35. Kastner-Klein P (1999) Experimentelle Untersuchung der strömungsmechanischen Transportvorgänge in Straßenschluchten. Diss Fakultät für Bauingeneur- und Vermessungswesen der Universität Karlsruhe (TH)
36. Kastner-Klein P, Plate EJ (1999) Wind-tunnel study of concentration fields in street canyons. Atmos Environ 33:3973–3979. doi:10.1016/S1352-2310(99)00139-9
37. Lawson R, Perry S, Thompson R (2000) Measurement of velocity and concentration fields in arrays of 2-dimensional and 3-dimensional buildings in a simulated neutrally-buoyant atmospheric boundary layer. USEPA FMF data report
38. Lim DW, Henn DS, Hookham PA (2001) Preliminary assessment of linked CFD operational dispersion models on the urban scale. Preprints. In: 3rd International symposium on environmental hydraulics, Tempe, AZ
39. McElroy JL (1969) A comparative study of urban and rural dispersion. J Appl Meteorol 8:19–31. doi:10.1175/1520-0450(1969)008<0019:ACSOUA>2.0.CO;2
40. Morris SC, Foss JF (2003) Turbulent boundary layer to single-stream shear layer: the transition region. J Fluid Mech 494:187–221. doi:10.1017/S0022112003006049
41. Moussafir J, Oldrini O, Tinarelli G, Sontowski J, Dougherty M (2004) A new operational approach to deal with dispersion around obstacles: the MSS (Micro Swift Spray) software system. In: 9th International conference on harmonisation within atmospheric dispersion modelling for regulatory purposes, Garmisch, Germany
42. Oke TR (1987) Boundary-layer climates, 2nd edn. Routledge, London
43. Pol SU, Bagal NL, Singh B, Brown MJ, Pardyjak ER (2006) Implementation of a new rooftop recirculation parameterization into the QUIC fast response urban wind model. Preprints. In: 6th AMS symposium urban environment, Atlanta, GA, CDROM JP2.1
44. Pope SB (2000) Turbulent flows. Cambridge University Press, Cambridge
45. Press WH, Teukolsky SA, Vetterling WT, Flannery BP (2007) Numerical recipes: the art of scientific computing, 3rd edn. Cambridge University Press, Cambridge
46. Pullen J, Boris JP, Young T, Patnaik G, Iselin J (2005) A comparison of contaminant plume statistics from a Gaussian puff and urban CFD model for two large cities. Atmos Environ 39:1049–1068. doi:10.1016/j.atmosenv.2004.10.043
47. Ramsdell JV, Fosmire CJ (1995) Atmospheric dispersion estimates in the vicinity of buildings. Report no PNL-10286, Pacific Northwest National Laboratory
48. Röckle R (1990) Bestimmung der Stromungsverhaltnisse im Bereich komplexer Bebauungsstrukturen. Ph.D. dissertation, Vom Fachbereich Mechanik, der Technischen Hochschule Darmstadt, Germany
49. Sasaki Y (1958) An objective analysis based on the variational method. J Meteorol Soc Jpn 36:77–88
50. Sasaki Y (1970) Some basic formalisms in numerical variational analysis. Mon Weather Rev 98:875–883. doi:10.1175/1520-0493(1970)098<0875:SBFINV>2.3.CO;2
51. Sasaki Y (1970) Numerical variational analysis formulated under the constraints as determined by longwave equations and a low-pass filter. Mon Weather Rev 98:884–898. doi:10.1175/1520-0493(1970)098<0884:NVAFUT>2.3.CO;2
52. Schulman L, Strimaitis D, Scire J (2000) Development and evaluation of the PRIME plume rise and building downwash model. J Air Waste Manag Assoc 50:378–390
53. Sherman CA (1978) A mass-consistent wind model for wind fields over complex terrain. J Appl Meteorol 17:312–319. doi:10.1175/1520-0450(1978)017<0312:AMCMFW>2.0.CO;2
54. Smith WS, Brown M (2002) A CFD generated wind field library feasibility study: maximum wind direction interval. Preprints. In: 4th AMS symposium urban environment, Norfolk, VA, Am Meteorol Soc 13.4
55. Snyder WH (1979) The EPA meteorological wind tunnel: its design, construction, and operating characteristics. Report no EPA-600/4-79-051, Environmental Protection Agency, Research Triangle Park, NC, 78 pp
56. Snyder WH (1981) Guideline for fluid modeling of atmospheric diffusion. Report no EPA-600/8-81-009, Environmental Protection Agency, Research Triangle Park, NC, 200 pp
57. Theurer W, Plate E, Hoeschele K (1996) Semi-empirical models as a combination of wind tunnel and numerical dispersion modeling. Atmos Environ 30:3583–3597. doi:10.1016/1352-2310(96)00072-6
58. Venkatram A, Isakov V, Pankratz D, Heumann J, Yuan J (2004) The analysis of data from an urban dispersion experiment. Atmos Environ 38:3647–3658. doi:10.1016/j.atmosenv.2004.03.045

59. Wang Y, Williamson C, Garvey D, Chang S, Cogan J (2005) Application of a multigrid method to a mass-consistent diagnostic wind model. J Appl Meteorol 44:1078–1089. doi:10.1175/JAM2262.1
60. Williams MD, Brown MJ, Boswell D, Singh B, Pardyjak ER (2004) Testing of the QUIC-PLUME model with wind-tunnel measurements for a high-rise building. Preprints. In: Fifth AMS symposium urban environment, Vancouver, BC, Am Meteorol Soc, CDROM J5.3
61. Wilson DJ (1979) Flow patterns over flat-roofed buildings and application to exhaust stack design. ASHRAE Trans 85:284–295
62. Wilson DJ, Chui EH (1994) Influence of building size on rooftop dispersion of exhaust gas. Atmos Environ 28:2325–2334. doi:10.1016/1352-2310(94)90486-3
63. Yamartino R, Strimaitis D, Messier T (1989) Modification of highway air pollution models for complex site geometries, vol 1, Data analyses and development of the CPB-3 model. Report no FHWA-RD-89-112